Mineralogical Magazine, April 2018, Vol. 82(2), pp. 375–399

Crystallization and destabilization of eudialyte-group minerals in peralkaline granite and pegmatite: a case study from the Ambohimirahavavy complex, Madagascar

GUILLAUME ESTRADE*, STEFANO SALVI AND DIDIER BÉZIAT

University of Toulouse, GET, CNRS, IRD, OMP, 14 Av. Edouard Belin, F-31400 Toulouse, France

[*Received 21 March 2016; Accepted 16 June 2017; Associate Editor: Katharina Pfaff*]

ABSTRACT

Eudialyte-group minerals (EGM) are very common in highly evolved SiO_2-undersaturated syenites and are characteristic minerals of agpaitic rocks. Conversely, they are extremely rare in peralkaline granites, with only a handful of EGM occurrences reported worldwide. Here, we study two new examples of EGM occurrence in two types of peralkaline pegmatitic granites from the Cenozoic Ambohimirahavavy complex, and assess the magmatic conditions required to crystallize EGM in peralkaline SiO_2-oversaturated rocks. In the transitional granite (contains EGM as accessory minerals) EGM occur as late phases and are the only agpaitic and major rare-earth element (*REE*) bearing minerals. In the agpaitic granite (contains EGM as rock-forming minerals) EGM are early-magmatic phases occurring together with two other agpaitic minerals, nacareniobsite-(Ce) and turkestanite. In these granites, EGM are partly-to-completely altered and replaced by secondary assemblages consisting of zircon and quartz in the transitional granite and an unidentified Ca-Na zirconosilicate in the agpaitic granite. Ambohimirahavavy EGM, as well as those from other peralkaline granites and pegmatites, are richer in *REE* and poorer in Ca than EGM in nepheline syenites. We infer that magmatic EGM are rare in SiO_2-oversaturated rocks because of low Cl concentrations in these melts. At Ambohimirahavavy, contamination of the parental magma of the agpaitic granite with Ca-rich material increased the solubility of Cl in the melt promoting EGM crystallization. In both granite types, EGM were destabilized by the late exsolution of a fluid and by interaction with an external Ca-bearing fluid.

KEYWORDS: eudialyte-group minerals, peralkaline granites, agpaitic rocks, zirconosilicate, high-field-strength elements, rare-earth elements, pegmatites.

Introduction

EUDIALYTE-group minerals (EGM) are complex Na-Ca-Zr-cyclosilicates with the general formula $Na_{15}(Ca,REE)_6(Fe,Mn)_3Zr_3Si(Si_{25}O_{72})(O,OH,H_2O)_3(Cl,OH)_2$ (Johnsen *et al.*, 2003) characteristic of evolved peralkaline [molar $(Na_2O+K_2O)/Al_2O_3>1$] SiO_2-undersaturated syenites, also called agpaitic syenites. This mineral is generally considered as diagnostic of agpaicity, i.e. those rocks in which high-field-strength elements (HFSE, such as Zr, Hf, Nb, Ta, U and Th) and rare-earth elements (*REE*) are incorporated into complex Na-K-Ca-Zr-silicates, rich in volatiles (Cl, F and H_2O) (Sørensen, 1992, 1997; Khomyakov, 1995; Le Maitre *et al.*, 2002; Marks *et al.*, 2011). By contrast, when HFSE are incorporated in more common minerals (e.g. zircon, titanite), rocks are termed miaskitic. EGM can contain important amounts of *REE* and are considered as a potentially valuable ore of *REE* and Zr (e.g. the Kringlerne deposit in the Ilímaussaq complex, the Norra Kärr complex in Sweden and the Kipawa complex in Canada; Goodenough *et al.* (2016) and Saucier *et al.* (2013)). Because EGM crystallize through a range of magmatic to hydrothermal conditions, their compositional variability can been used to monitor the conditions of the environment in which they crystallized

*E-mail: Estrade.guillaume@gmail.com
https://doi.org/10.1180/minmag.2017.081.053

(Mitchell and Liferovich, 2006; Schilling *et al.*, 2009; Marks *et al.*, 2015; Ratschbacher *et al.*, 2015). Very commonly, EGM are partly-to-completely replaced by secondary phases, at late magmatic-to-hydrothermal stages (Salvi *et al.*, 2000; Mitchell and Liferovich, 2006; Karup-Møller *et al.*, 2010; Sheard *et al.*, 2012; Karup-Møller and Rose-Hansen, 2013).

Although EGM were considered initially to be characteristic of highly differentiated SiO_2-undersaturated rocks, these minerals have also been reported in a few SiO_2-oversaturated peralkaline rocks. The only known examples, to our knowledge, are: quartz syenite from the Carlingford complex, Ireland (Nockolds, 1950); the Pajarito mountain, Texas (McLemore, 2015); granitic dykes from the Ascension Island in the South Atlantic (Harris *et al.*, 1982); the Straumsvola complex in Antarctica (Harris and Rickard, 1987); the Windy Fork pluton in Alaska (Gunter *et al.*, 1993); pegmatitic granitic dykes from the Ambohimirahavavy complex in Madagascar (Estrade *et al.*, 2014*a*); the Dara-i-Pioz massif in Tajikistan (Grew *et al.*, 1993); Rockall Island in the North Atlantic (Sabine, 1957). However, in studies of most of these occurrences, EGM are only mentioned as an accessory mineral and are not thoroughly described in terms of texture and composition, although in their recent compilation, Schilling *et al.* (2011) characterized the EGM from Ascension Island and Straumsvola.

In place of EGM, other magmatic complex Zr-silicates are usually described in peralkaline granites and pegmatites (Table 1). The most commonly reported Zr-minerals include dalyite ($K_2ZrSi_6O_{15}$), wadeite ($K_2ZrSi_3O_9$), elpidite ($Na_2ZrSi_6O_{15}\cdot 3H_2O$), catapleiite ($Na_2ZrSi_3O_9\cdot 2H_2O$) and, more rarely, gittinsite ($CaZrSi_2O_7$) and armstrongite ($CaZrSi_6O_{15}\cdot 2H_2O$). It is noteworthy that, among these six minerals, none contain Cl or F, whereas three contain H_2O (elpidite, catapleiite and armstrongite). Several Zr-minerals are usually reported in the same peralkaline rocks and their complex textural relationships have often led to multiple interpretations (e.g. Strange Lake, Birkett *et al.*, 1992; Roelofsen and Veblen, 1999). Moreover, in many cases, post-magmatic processes have destabilized the primary assemblages, substantially complicating identification of the original magmatic mineralogy.

The main factors controlling the saturation of EGM in a melt are its peralkalinity and high HFSE (mainly Zr) and volatile contents (mainly Cl, F and H_2O) (Sørensen, 1997). These conditions are usually met in highly-evolved undersaturated melts derived from the differentiation of magmas under low oxygen fugacity (Markl *et al.*, 2010). Conversely, the problem of scarcity of EGM in peralkaline granites has, to date, not been discussed in the literature.

This study focuses on the occurrence of EGM in peralkaline granitic pegmatites in the Ambohimirahavavy alkaline complex, northwest Madagascar. On the basis of textural and compositional data for EGM, other agpaitic minerals, clinopyroxene and amphibole, we assess the magmatic conditions required for the stability of EGM in peralkaline SiO_2-oversaturated rocks and compare them to their undersaturated counterpart.

Geological setting and petrography

The Ambohimirahavavy alkaline complex (24.2 ± 0.6 Ma for nepheline syenite and 23.5 ± 6.8 Ma for peralkaline granite; *in situ* U–Pb radiometric age determination of zircon, Estrade *et al.*, 2014*b*) is part of the Cenozoic alkaline province located in the north-western part of Madagascar, in the Ampasindava peninsula. The complex consists of silica-undersaturated and silica-oversaturated syenites and granites as well as volcanic units of alkaline affinity, including basalt, phonolite, trachyte and rhyolitic obsidian (Fig. 1). A network of granitic and pegmatitic dykes intruded the Isalo sedimentary units along the external flank of the south syenitic ring-dyke. The dykes are characterized by an alkaline mineralogy (i.e. contain sodic clinopyroxene and sodic amphibole) and by the presence of minerals rich in HFSE and *REE*. Their local intrusion in limestone resulted in the formation of a *REE*-rich skarn (Estrade *et al.*, 2015).

This complex is currently being explored by Tantalus Rare Earth AG, with a focus on the ion-adsorption *REE* mineralization in clays associated with laterites. The company has also evaluated the economic potential of the bedrock, as most of the HFSE and *REE* occur as primary mineralization in peralkaline granite and pegmatite dykes. In a previous study, we distinguished three types of dykes according to their textures and major mineralogy (Estrade *et al.*, 2014*a*): (1) A coarse-grained granitic type (GR-I), characterized by an allotriomorphic granular texture, composed of quartz, perthitic alkali feldspar, Na-amphibole and Na-clinopyroxene. The main HFSE-bearing minerals form a miaskitic assemblage consisting of zircon, pyrochlore-group minerals, monazite-(Ce)

https://doi.org/10.1180/minmag.2017.081.053 Published online by Cambridge University Press

TABLE 1. List of the main Zr-silicates in agpaitic peralkaline granite and pegmatite.

Zr-silicate	Formula	Locality	Mode of occurrence	Replaced mineral	Reference
Ca-phases					
Gittinsite	$CaZrSi_2O_7$	Kaldzan Buregte	Late to post-magmatic		[8]
		Strange Lake	Post-magmatic	Armstrongite	[1]; [15]; [14]
		Khan Bogd	Post-magmatic	Elpidite	[10]
Armstrongite	$CaZrSi_6O_{15}.2H_2O$	Strange Lake	Magmatic and post-magmatic	Elpidite	[1]; [15]; [14]
		Khan Bogd	Post-magmatic	Elpidite	[10]
Na-phases					
Elpidite	$Na_2ZrSi_6O_{15}.3H_2O$	Kaldzan Buregte	Late to post-magmatic		[8]
		Strange Lake	Magmatic and post-magmatic		[1]; [15]; [14]
		Khan Bogd	Early-magmatic and post-magmatic	Elpidite	[10]
		Ilímaussaq	?		[12]
Catapleiite	$Na_2ZrSi_3O_9.2H_2O$	Strange Lake	Magmatic and post-magmatic		[1]
		Kaldzan Buregte	Late to post-magmatic		[8]
Vlasovite	$Na_2ZrSi_4O_{11}$	Strange Lake	Magmatic		[1]
		Ascension Island	Magmatic		[3]; [6]
K-phases					
Dalyite	$K_2ZrSi_6O_{15}$	Strange Lake	Magmatic		[1]
		Straumsvola	Magmatic		[7]
		Ascension Island	Magmatic		[5]
		Amis	Late-magmatic		[16]
Wadeite	$K_2ZrSi_3O_9$	Strange Lake	Magmatic and post-magmatic		[1]
Eudialyte	$Na_{15}Ca_6Fe_3Zr_3Si(Si_{25}O_{73})(O,OH,H_2O)_3(Cl,OH)_2$	Ambohimirahavavy	Early and late-magmatic		[2], this study
		Straumsvola	Magmatic		[7]
		Ascension Island	Magmatic		[5]
		Dara-i-pioz	Magmatic		[4] ; [9]
		Carlingford	Magmatic		[13]
		Pajarito	Magmatic		[17]; [11]
Zircon	$ZrSiO_4$	Ambohimirahavavy	Magmatic and post-magmatic	EGM	[2]
		Strange Lake	Post-magmatic	Armstrongite–gittinsite	[1]; [15]; [14]
		Khan Bogd	Post-magmatic	Elpidite	[10]

References: [1] Birkett *et al.* (1992); [2] Estrade *et al.* (2014*a*); [3] Fleet and Cann (1967) [4] Grew *et al.* (1993); [5] Harris *et al.* (1982); [6] Harris (1983); [7] Harris and Rickard (1987); [8] Kempe *et al.* (2015); [9] Khomyakov *et al.* (2003); [10] Kynicky *et al.* (2011); [11] Mariano, *Pers. Comm.*; [12] Marks *et al.* (2015); [13] Nockolds (1950); [14] Roelofsen and Veblen (1999); [15] Salvi and Williams-Jones (1995); [16] Schmitt *et al.* (2002); [17] Sherer (1990).

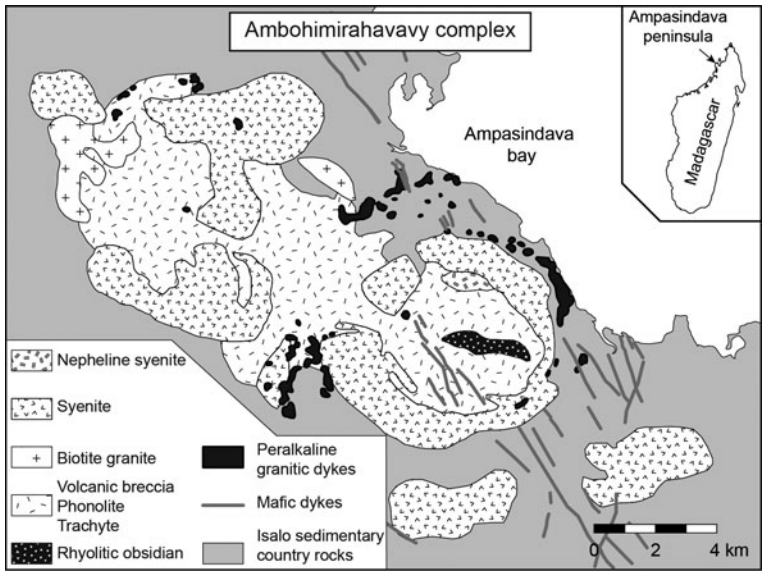

FIG. 1. Geological map of the Ambohimirahavavy complex, modified after Donnot (1963).

and chevkinite-(Ce). (2) A pegmatitic granitic type (GR-II), consisting of quartz, perthitic alkali feldspar, Na-clinopyroxene, Na-amphibole, and containing an agpaitic to miaskitic accessory assemblage consisting of EGM, mostly altered to a secondary miaskitic assemblage that is dominated by zircon and quartz (Fig. 2*a*,*b*,*c*). This rock is termed transitional because of this feature and because EGM only occur as accessory minerals. (3) A pegmatitic agpaitic granitic type (GR-III) that consists of K-feldspar, albite, Na-clinopyroxene, Na-amphibole and quartz, plus EGM as rock-forming minerals (Fig. 2*d*–*e*). Other agpaitic minerals include nacareniobsite-(Ce) (Na_3Ca_3(Ce, La)(Nb,Ti)$(Si_2O_7)_2OF_3$) and turkestanite (Th(Ca, $Na)_2K_{1-x}\square_x(Si_8O_{20})\cdot nH_2O$).

In the following sections, we describe in detail the EGM and the complex mineralogy of both the pegmatitic transitional (GR-II) and the pegmatitic agpaitic (GR-III) dykes. These dykes form a more-or-less continuous belt around the ring-dyke of syenite. They vary in thickness from a few centimetres to a few metres. Although no relationships have been observed between GR-II and GR-III dykes, their similar mode of emplacement suggests a contemporaneous origin. GR-II dykes are far more common in the complex than GR-III, which have been only found in boreholes. However, Lacroix (1915, 1923) and Ganzeev and Grechishchev (2003) have described similar rocks to GR-III dykes containing more than 40% of EGM, suggesting that they outcrop somewhere in the flank of the complex.

Analytical methods

The mineralogy and textural relationships were investigated using optical microscopy and back-scattered electron (BSE) imaging using a JEOL JSM 6360LV scanning electron microscope (SEM) equipped with a silicon drift detector analysis system. The instrument was also used to obtain energy-dispersive X-ray phase maps.

Major and minor element concentrations in minerals were determined using a Cameca-SX-50 electron probe microanalyser (EPMA) with SAMx automation, at the Géosciences Environment Toulouse (GET) laboratory at the University of Toulouse. Operating conditions were an accelerating voltage of 15 kV and a beam current of 20 nA. Standardization was obtained using, periclase (Mg), wollastonite (Ca and Si), corundum (Al), pyrophanite (Mn and Ti), hematite (Fe), baryte (Ba), albite (Na), sanidine (K), zircon (Hf and Zr), graftonite (P), UO_2 (U), ThO_2 (Th), $Pb_2P_2O_7$ (Pb), sphalerite (Zn), orthophosphate for *REE* and yttrium, Nb metal (Nb), Ta metal (Ta), topaz (F) and tugtupite (Cl).

In situ trace-element concentrations were determined by laser ablation inductively coupled plasma

https://doi.org/10.1180/minmag.2017.081.053 Published online by Cambridge University Press

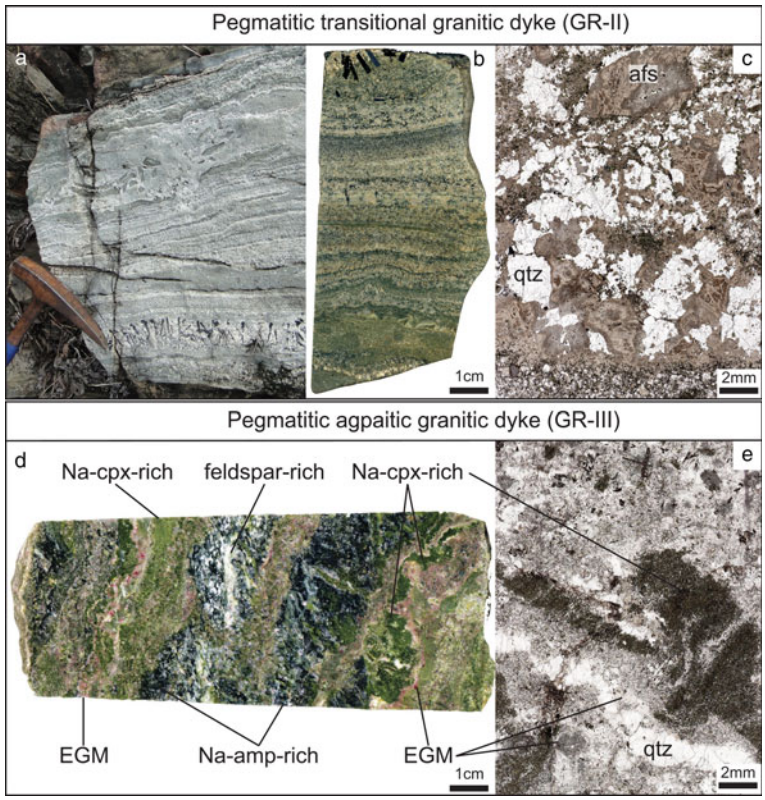

FIG. 2. Outcrop photograph (*a*), scanned polished rock slab (*b–d*) and scanned thin sections (*c–e*) of the pegmatitic transitional granitic dyke (GR-II) (*a*, *b*, *c*) and pegmatitic agpaitic granitic dyke (GR-III) (*d*, *e*). Both rock types show pronounced layering and variable grain sizes typical of pegmatite. Abbreviations: afs: alkali feldspar, amp: amphibole, cpx: clinopyroxene and qtz: quartz.

mass-spectrometry (LA-ICP-MS) at the University of Montpellier. The instrument used for analysis was a Geolas Q excimer CompEx 102 laser ablation system coupled to a ThermoFinnigan Element XR ICP-MS. We used a beam diameter of 60 µm for all analyses, which allowed a high detection threshold even for very low-level trace elements. For each analysis, the signal was recorded for 180 s, consisting of 60 s of background measurement followed by 120 s of ablation. To calibrate the instrument, we used NIST SRM 610 glass as an external standard and NIST SRM 612 as a secondary standard. SiO_2 was used as an internal standard for the correction of different ablation rates between sample and standard. Silica concentration had been determined previously by EPMA in the ablation area. Data processing was carried out with the *SILLS* software (Guillong *et al.*, 2008). Typical concentration uncertainties are ± 5% for concentrations >10 µg/g and ± 10% for concentration <10 µg/g.

Mineral textures and alteration

Eudialyte-group minerals

In GR-II, EGM are accessory minerals (<1 vol.%) occurring as interstitial, late-formed magmatic phases surrounded by Na-clinopyroxene, Na-amphibole, perthitic alkali feldspars and quartz (Fig. 3*a–b*). In most samples, EGM underwent partial-to-complete alteration and have been replaced by a complex assemblage of secondary minerals, among which zircon and quartz have been identified as the main replaced phases (Estrade *et al.*, 2014*a*). Although most of the EGM grains are altered, rare, entirely unaffected grains may occur adjacent to altered ones. The latter crystals lack the oscillatory growth or sector zoning usually observed in EGM from other alkaline complexes, although high-contrast BSE images show common small bright phases and dark grey patches, scattered along fractures.

https://doi.org/10.1180/minmag.2017.081.053 Published online by Cambridge University Press

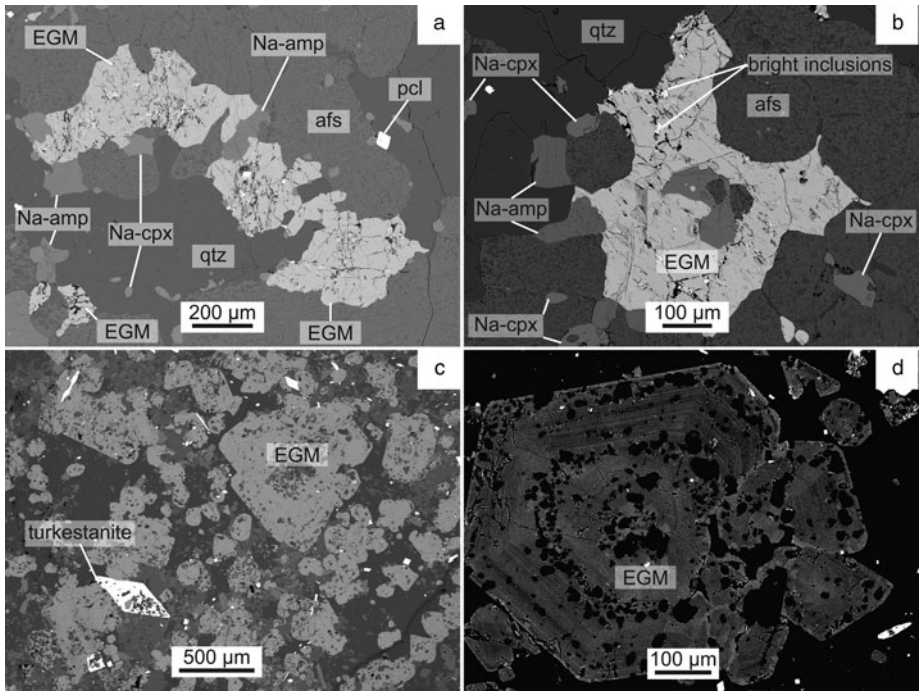

FIG. 3. BSE images of EGM textures from GR-II (*a–b*) and GR-III (*c–d*): (*a–b*) Late-magmatic interstitial EGM partially altered along fractures. (*c–d*) Oscillatory-zoned early-magmatic euhedral EGM with mineral inclusions. Abbreviations: afs: alkali feldspar; amp: amphibole; cpx: clinopyroxene; qtz: quartz; pcl: pyrochlore.

In GR-III, EGM are rock-forming minerals (>10 vol.%) occurring as euhedral, early magmatic crystals together with Na-clinopyroxene, Na-amphibole, nacareniobsite-(Ce), turkestanite, albite, K-feldspar and quartz (Fig. 3*c–d*). Except for quartz, all these minerals occur as individual grains and as inclusions in cores of the EGM, as well as along concentric layers that follow growth zones. Quartz mainly occurs as late anhedral crystals and as layers flanked by euhedral eudialyte. Unlike in GR-II, most of the EGM are pristine; locally-altered EGM grains occur in narrow bands, together with calcite, altered nacareniobsite-(Ce) and turkestanite. All other silicates were not altered.

Other agpaitic minerals

In addition to EGM, the agpaitic minerals nacareniobsite-(Ce) and turkestanite occur in significant modal amounts (1–2 vol.%) in GR-III, whereas EGM are the only agpaitic minerals in GR-II. Nacareniobsite-(Ce) is also a mineral typical of agpaitic SiO_2-undersaturated rocks, but has been only rarely described in SiO_2-saturated rocks (Vilalva *et al.*, 2013). In GR-III, it occurs as early magmatic elongated euhedral crystals that enclose small chadacrysts of albite, K-feldspar, Na-clinopyroxene and Na-amphibole (Fig. 4*a–b*). In altered portions of GR-III, nacareniobsite-(Ce) is replaced by a complex assemblage of secondary Ca-rich minerals including calcite and titanite. Turkestanite is an extremely rare mineral that has been reported in only four other alkaline complexes (Pautov *et al.*, 1997; Kabalov *et al.*, 1998; Vilalva and Vlach, 2010). In GR-III, it is an early magmatic phase, occurring as diamond-shaped euhedral crystals that enclose small chadacrysts of albite, K-feldspar, Na-clinopyroxene and Na-amphibole (Fig. 4*c*). In BSE images, these crystals commonly show zoning and alteration textures consisting of a heterogeneous core containing a network of very thin U-rich veinlets, surrounded by a BSE brighter homogeneous rim (Fig. 4*d*).

Na-clinopyroxene and Na-amphibole

Sodic clinopyroxene is the main mafic constituent in GR-II and GR-III. In GR-II, it forms two

https://doi.org/10.1180/minmag.2017.081.053 Published online by Cambridge University Press

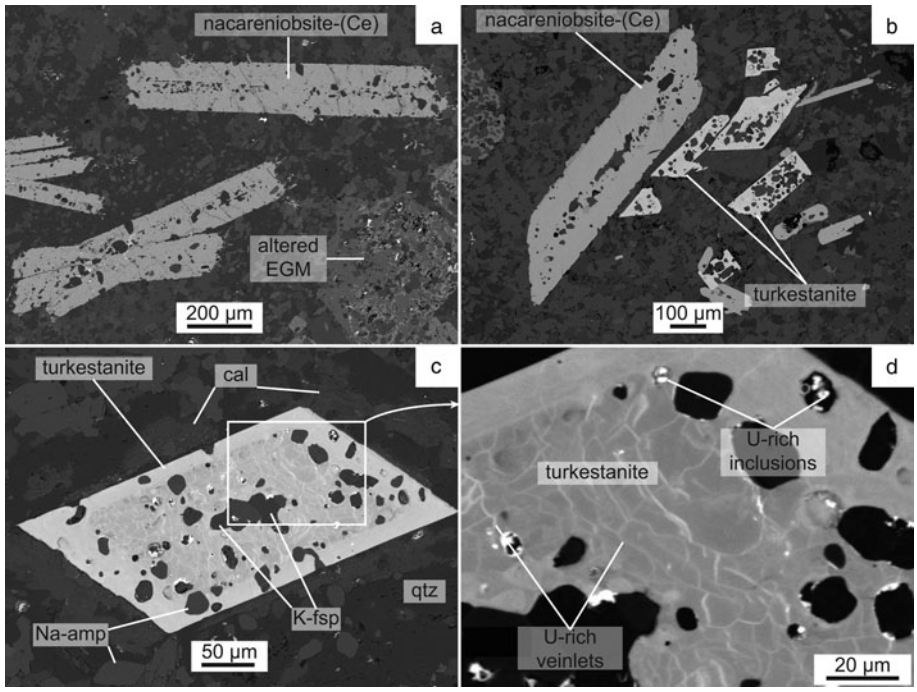

FIG. 4. BSE images of agpaitic minerals in GR-III: (*a–b*) euhedral laths of nacareniobsite-(Ce) containing mineral inclusions. (*c–d*) zoned euhedral turkestanite containing mineral inclusions. The core of the turkestanite shows bright U-rich veinlets and inclusions. Abbreviations: amp: amphibole; cal: calcite; K-fsp: K-feldspar; qtz: quartz.

texturally distinct generations: Na-clinopyroxene-I (cpx-I) is relatively uncommon and forms large euhedral phenocrysts (up to 1 mm across), locally showing distinct cores and rims; Na-clinopyroxene-II (cpx-II) is more abundant and occurs as homogeneous small grains or thin acicular crystals. In GR-III, Na-clinopyroxene occurs as small euhedral crystals and as chadacrysts in EGM, nacareniobsite-(Ce) and turkestanite.

Sodic amphibole is the second main mafic constituent after Na-clinopyroxene. In GR-II, its habit varies considerably and, depending on its location in the dyke, can form large euhedral pegmatitic crystals of up to 20 cm or small anhedral grains. In GR-III, Na-amphibole occurs only as small euhedral crystals.

Mineral composition

Eudialyte-group minerals

Representative compositions of EGM are shown in Table 2. Structural formulae of EGM are based on Σ (Si + Al + Zr + Ti + Hf + Nb) = 29 atoms per formula unit (apfu) and were calculated using the Excel spreadsheet of Pfaff *et al.* (2010). EGM from GR-II and GR-III have different compositions, mainly in Mn, Ca and *REE*, and minor variations in Si, Fe, Na and Nb. Zirconium and chlorine contents of EGM are similar in both rock types. Binary plots of Fe vs. Mn and (La + Ce + Nd + Y) vs. Ca, expressed as atoms per formula unit, are shown in Fig. 5, where they are compared with EGM from other peralkaline granites (Straumsvola and Ascension Island) and foid syenites (Ilímaussaq, Mont Saint-Hilaire, Tamazeght, Pilansberg, Kipawa, Khibiny, Lovozero, Saima, Pocos de Caldas, Langesundfjord and Norra Kärr) using the data of Schilling *et al.* (2011). The Mn content of early-magmatic EGM from GR-III is lower than that of late-magmatic EGM from GR-II and is consistent with data from the other complexes, showing that, in a single intrusive complex, the Mn/Fe ratio increases in later-formed EGM (Schilling *et al.*, 2011). Calcium correlates negatively with the sum of the major *REE*s: La, Ce, Nd and Y; this trend is consistent with their preferential incorporation in

https://doi.org/10.1180/minmag.2017.081.053 Published online by Cambridge University Press

TABLE 2. Average compositions of EGM and their replacing phases in pegmatitic transitional (GR-II) and pegmatitic agpaitic (GR-III) dykes.

Dyke type	Pegmatitic transitional (GR-II)						Pegmatitic agpaitic (GR-III)						Formulae based on (Si + Al + Zr + Ti + Hf + Nb) = 29				
	EGM (Fig. 3*a–b*)		Ca-zirconosilicate (Fig. 8)		Zircon (Fig. 8)		EGM (Fig. 3*c–d*)		Intermediate phase (Fig. 9*b*)		Ca-Na zircono-silicate (Fig. 9*a–b*)			GR-II EGM		GR-III EGM	
Mineral																	
NA*	18	σ	10	σ	5	σ	12	σ	3	σ	4	σ		18	σ	12	σ
SiO_2	46.15	0.91	40.28	0.48	30.04	0.56	50.22	1.51	54.02	1.64	63.63	0.82	Si	25.25	0.08	25.79	0.09
TiO_2	0.41	0.25	b.d.l.	–	n.a.	–	0.18	0.24	b.d.l.	–	b.d.l.	–	Ti	0.17	0.28	0.07	0.36
ZrO_2	10.61	0.12	33.29	0.45	57.77	1.58	10.94	0.31	10.92	0.18	19.70	0.69	Zr	2.83	0.09	2.74	0.18
HfO_2	0.17	0.06	0.83	0.10	1.04	0.09	0.13	0.05	0.16	0.02	0.32	0.11	Hf	0.03	0.01	0.02	0.01
Al_2O_3	0.00	0.00	1.11	0.21	b.d.l.	–	0.00	0.00	b.d.l.	–	b.d.l.	–	Al	0.00	0.00	0.00	0.00
Nb_2O_5	2.92	0.04	b.d.l.	–	n.a.	–	1.63	0.03	1.59	0.23	b.d.l.	–	Nb	0.72	0.03	0.38	0.02
La_2O_3	1.57	0.12	b.d.l.	–	n.a.	–	1.21	0.17	1.18	0.19	b.d.l.	–	La	0.32	0.05	0.23	0.07
Ce_2O_3	3.06	0.06	0.22	0.12	0.57	0.32	2.62	0.07	2.29	0.25	b.d.l.	–	Ce	0.61	0.05	0.49	0.06
Nd_2O_3	1.16	0.17	0.19	0.15	n.a.	–	1.01	0.16	n.a.	–	n.a.	–	Nd	0.23	0.12	0.19	0.07
Sm_2O_3	0.31	0.22	b.d.l.	–	n.a.	–	0.28	0.22	0.35	0.06	b.d.l.	–	Sm	0.03	0.06	0.03	0.05
Gd_2O_3	0.58	0.20	b.d.l.	–	n.a.	–	0.29	0.10	0.23	0.17	b.d.l.	–	Gd	0.05	0.04	0.02	0.02
Y_2O_3	3.61	0.23	0.19	0.09	1.13	1.01	1.60	0.35	1.54	0.04	1.44	0.25	Y	1.05	0.05	0.44	0.11
FeO	3.76	0.09	1.13	0.15	0.65	0.13	4.24	0.14	3.36	0.37	0.14	0.08	Fe	1.72	0.02	1.82	0.03
MnO	5.66	0.15	1.37	0.18	n.a.	–	1.88	0.16	2.00	0.09	b.d.l.	–	Mn	2.62	0.03	0.82	0.03
CaO	3.97	0.07	14.98	0.41	0.09	0.07	7.74	0.10	8.65	0.47	2.36	0.17	Ca	2.33	0.02	4.26	0.02
PbO	n.a.	–	1.15	0.27	b.d.l.	–	n.a.	–	0.25	0.11	b.d.l.	–	Na	9.57	0.01	11.35	0.01
Na_2O	9.02	0.13	b.d.l.	–	n.a.	–	11.39	0.12	10.19	0.35	2.60	0.19	K	0.39	0.02	0.27	0.02
K_2O	0.56	0.21	b.d.l.	–	n.a.	–	0.41	0.21	0.32	0.02	b.d.l.	–	Cl	1.73	0.04	1.55	0.02
UO_2	n.a.	–	b.d.l.	–	b.d.l.	–	n.a.	–	0.12	0.05	b.d.l.	–	Sum	47.92	0.42	48.92	0.53
Cl	1.87	0.09	b.d.l.	–	n.a.	–	1.78	0.05	1.79	0.06	b.d.l.	–					
O = Cl	0.42	0.01	–	–	–	–	0.40	0.01	–	–	–	–					
Total	94.95	1.17	94.74	0.75	91.49	1.09	97.18	2.08	98.94	1.64	90.19	1.18					

Abbreviations: EGM = eudialyte-group minerals, b.d.l. = below detection limit, n.a. = not analysed, σ = standard deviation
*NA – number of analyses

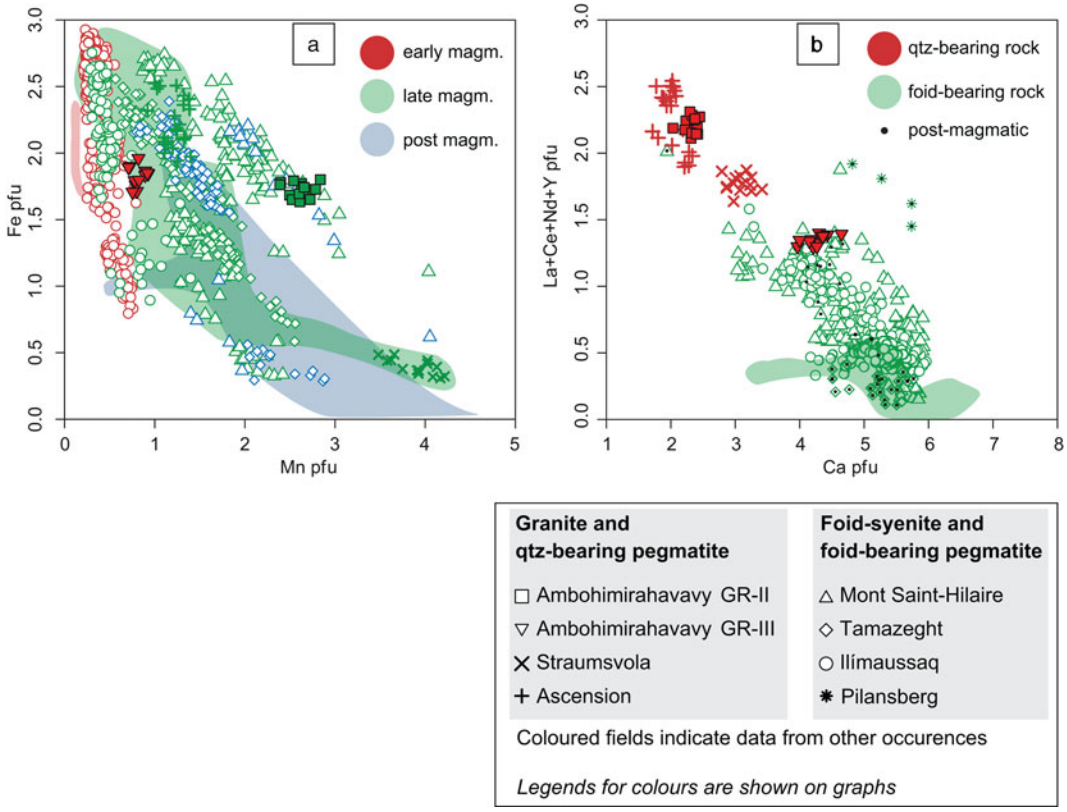

FIG. 5. (*a*) A plot of Fe *vs.* Mn in atom per formula units of EGM from the Ambohimirahavavy complex (filled symbols) compared with EGM from other alkaline complexes taken from Schilling *et al.* (2011). (*b*) A plot of La + Ce + Nd + Y *vs.* Ca in atom per formula units of EGM from the Ambohimirahavavy complex (filled symbols) compared with EGM from other alkaline complexes taken from Schilling *et al.* (2011).

the same structural site (M1; Johnsen and Grice, 1999). In addition, most of the EGM from quartz-bearing rocks (GR-II, Straumsvola and Ascension Island) have lower Ca and higher La + Ce + Nd + Y contents than EGM from foid-bearing rocks. Most EGM with high La + Ce + Nd + Y content from foid-bearing rocks (Mont Saint-Hilaire and Pilansberg) have a post-magmatic origin.

Trace-element analyses for EGM, agpaitic minerals, clinopyroxene and amphibole are presented in an electronic supplement. Rare-earth elements and trace-element distribution patterns of EGM, nacareniobsite-(Ce), turkestanite, clinopyroxene and amphibole are shown in Fig. 6. Rare-earth element and trace-element patterns of EGM are compared with patterns of EGM from other EGM-bearing granites (Straumsvola and Ascension Island) and foid-syenites using the data of Schilling *et al.* (2011). We only present the patterns from the most *REE*-rich EGM (from Ilímaussaq and Mont Saint-Hilaire), as EGM from other complexes plot far below the *REE* distribution patterns of GR-II and GR-III. We also compare the concentrations of the light *REE* (*LREE*; La to Sm) and the heavy *REE* (*HREE*; Gd to Lu) in EGM from different complexes in Fig. 7 using the data of Schilling *et al.* (2011). Among all EGM, those from quartz bearing-rocks have the highest *REE* concentrations and are generally enriched by up to four orders of magnitude relative to chondrite (McDonough and Sun, 1995) (Fig. 6*a*). Concentrations of the *LREE* in EGM from quartz bearing-rocks (>40,000 ppm) are similar to the most *LREE*-rich EGM from foid-syenites in Ilímaussaq and Mont Saint-Hilaire, whereas concentrations of the *HREE* are significantly higher in EGM from GR-II and Ascension Island (Fig. 7). All patterns show a strong negative

https://doi.org/10.1180/minmag.2017.081.053 Published online by Cambridge University Press

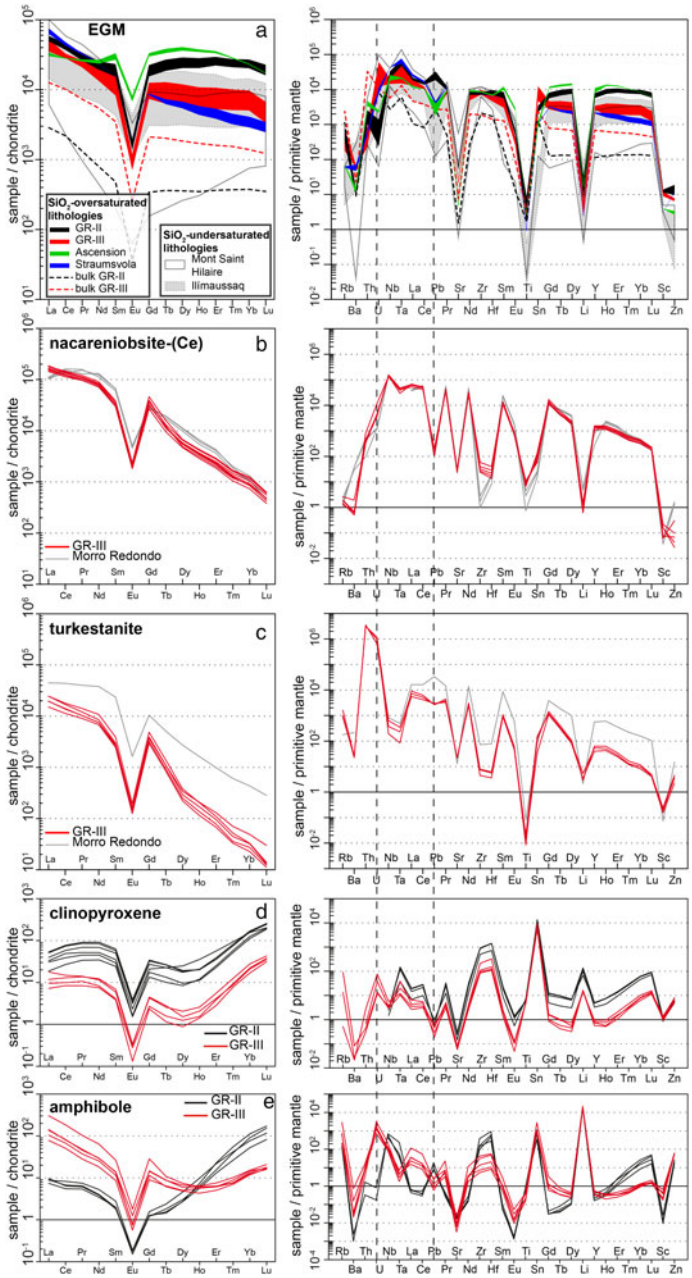

FIG. 6. Chondrite normalized *REE* (left) and trace-element (right) distribution patterns from (*a*) EGM, (*b*) nacareniobsite-(Ce), (*c*) turkestanite, (*d*) clinopyroxene and (*e*) amphibole. EGM patterns from GR-II and GR-III are compared with whole-rock patterns from GR-II and GR-III (dashed lines) using data from Estrade *et al.* (2014*b*; GR-II dyke type sample AM113A) and Estrade *et al.* (2014*a*; GR-III dyke type sample EU01). EGM patterns are also compared with EGM data from other alkaline complexes taken from Schilling *et al.* (2011) (cf. legend). Nacareniobsite-(Ce) and turkestanite patterns are compared with data from the Morro Redondo complex (Brazil) taken from Vilalva and Vlach (2010) and Vilalva *et al.* (2013).

https://doi.org/10.1180/minmag.2017.081.053 Published online by Cambridge University Press

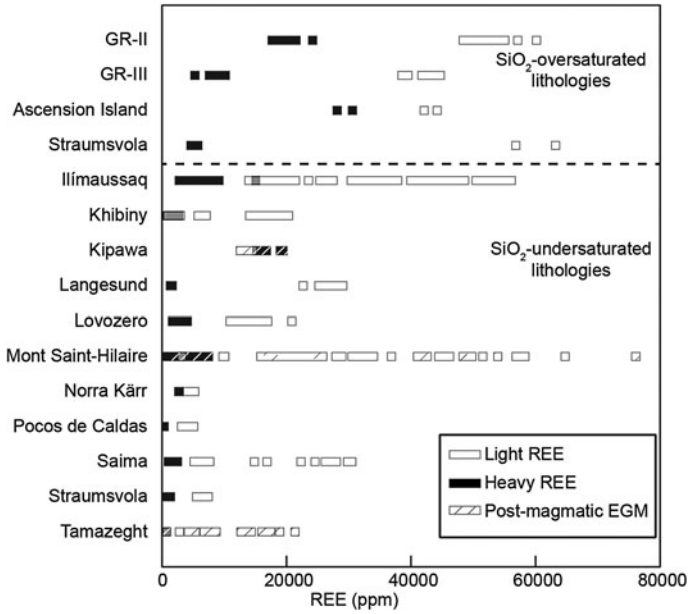

FIG. 7. Range of light (La to Sm) and heavy (Gd to Lu) *REE* concentrations in EGM from the Ambohimirahavavy complex and other alkaline complexes. Data for other complexes are from Schilling *et al.* (2011). The grey colour indicates overlap of the white and black patterns in the legends.

Eu anomaly which is also a characteristic of the whole-rock *REE* distribution patterns of the dykes; this is consistent with the model for the origin of the melt in the Ambohimirahavavy complex (Estrade *et al.*, 2014*b*), i.e. differentiation of an alkali basaltic parental melt by fractionation of plagioclase. Trace-element distribution patterns have similar overall shapes, except for U and Pb, which show a negative and positive anomaly, respectively, in GR-II, and an opposite pattern in GR-III. Such opposed trends are absent in the whole-rock patterns, which show similar concentrations for these two elements.

Alteration paragenesis of EGM

Most of the EGM in GR-II samples are replaced entirely by a secondary paragenesis, consisting ultimately of zircon and quartz. Locally, however, EGM are partly altered and replaced by an assemblage of Zr-Ca-bearing phases and *REE*-Ca-F-bearing phases with no zircon (Estrade *et al.*, 2014*a*). In the present work, we have identified EGM that show partial replacement by zircon, and we consider this texture as representative of the alteration pattern of EGM in GR-II. An X-ray element map of partially-replaced EGM is shown in Fig. 8 and the compositions of the phases present are reported in Table 2. In this Figure, EGM are replaced ultimately by zircon and quartz through an intermediate step consisting of an unidentified Ca-zirconosilicate with higher Ca and Zr and lower Fe and Mn contents than the original EGM. All Na, Cl, Nb and most of the *REE* have been lost. *REE*-rich and Zr-rich phases co-crystallized with the Ca-zirconosilicate but were not analysed with EPMA due to their very small size. Secondary zircon is characterized by a low ZrO_2 content (57.8 wt.%), a low sum of oxides (91.5 wt.%) and the presence of Fe and Ca. In GR-III, replacement of EGM involved an intermediate phase slightly enriched in Si (Fig. 9*a–b*). The replacing phase is an unidentified Ca-Na zirconosilicate lacking Cl, *REE*, Mn and Fe.

Other agpaitic minerals

Representative compositions of nacareniobsite-(Ce) and turkestanite are given in Table 3. The compositions of different grains of nacareniobsite-(Ce) are similar and comparable to that of nacareniobsite-(Ce) published for other complexes

https://doi.org/10.1180/minmag.2017.081.053 Published online by Cambridge University Press

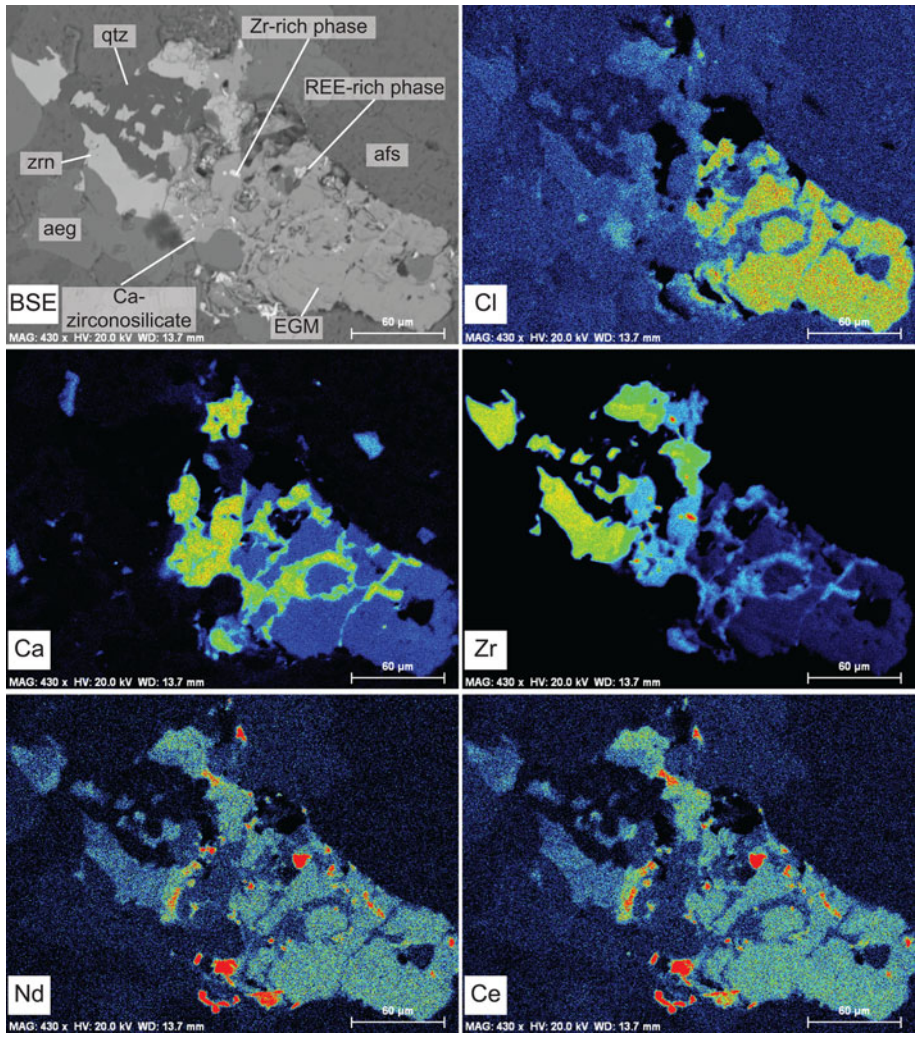

FIG. 8. BSE image and X-ray maps depicting the distribution of chlorine (Cl), calcium (Ca), zirconium (Zr), neodymium (Nd) and cerium (Ce), showing partial replacement of EGM (BSE image lower right hand side) by zircon and quartz (BSE image left hand side) in GR-II. Replacement takes place through formation of an intermediate Ca-zirconosilicate with Zr-rich and *REE*-rich phases. Abbreviations: aeg: aegirine; afs: alkali feldspars; qtz: quartz; and zrn: zircon.

(Sokolova and Hawthorne, 2008; Vilalva *et al.*, 2013; Borst *et al.*, 2016). Fluorine content is higher than in the ideal formulae, as the calculated cations at ~3.7 apfu exceed the ideal value of 3 cations. The *REE* distribution patterns show a steep negative slope from *LREE* to *HREE*, similar to published patterns (Vilalva *et al.*, 2013) (Fig. 6*b*). Trace-element distribution patterns reproduce the strong negative anomalies for Sr, Ti and Li that characterize EGM. Alteration products consist mainly of calcite, titanite and quartz (Fig. 9*c–d*).

Turkestanite is characterized by a low sum of oxides (88–95 wt.%) and by compositional differences between crystals and between core and rim of altered crystals (Fig. 9*e–f*). The low total oxide sum is consistent with most of the compositions reported in the literature, and is probably related to structural H_2O, not analysed with EPMA (Pautov *et al.*, 1997; Vilalva and Vlach, 2010). However, the very low sum of oxides of altered cores could result from porosity created by alteration processes and subsequent loss of volume. Altered cores are

https://doi.org/10.1180/minmag.2017.081.053 Published online by Cambridge University Press

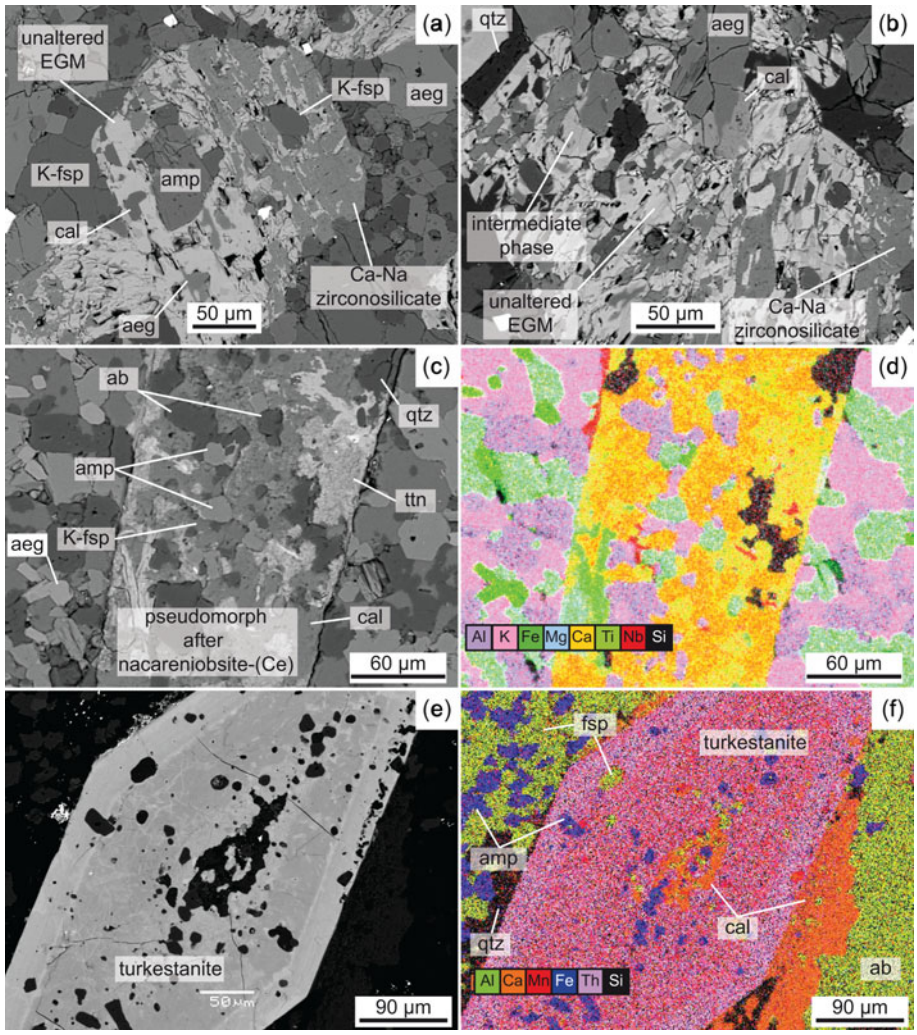

FIG. 9. BSE images (*a*, *b*, *c* and *e*) and false-coloured X-ray maps (*d*, *f*) of altered agpaitic minerals in GR-III: (*a–b*) altered EGM replaced by Ca-Na zirconosilicate, an intermediate phase and calcite; (*c–d*) altered nacareniobsite-(Ce) replaced mainly by calcite and titanite; and (*e–f*) zoned altered turkestanite with calcite. Abbreviations: ab: albite; aeg: aegirine; amp: amphibole; cal: calcite; K-fsp: K-feldspar; qtz: quartz; ttn: titanite.

characterized by lower Si, Th, Na and K and higher Mn content compared to their rims and the unaltered crystals. Similarly to nacareniobsite-(Ce), *REE* distribution patterns show a steep negative slope from *LREE* to *HREE*, not unlike the patterns given by Vilalva and Vlach (2010) (Fig. 6*c*).

Na-clinopyroxene and Na-amphibole

Further insights into the crystallization processes can be obtained by studying the detailed chemical changes of other rock-forming, non-agpaitic minerals, which are also liable to incorporate HFSE and *REE*. Representative compositions of Na-clinopyroxene and Na-amphibole in GR-II and GR-III are reported in Tables 4 and 5. Structural formulae of clinopyroxene are based on four cations and six oxygens and those of amphibole have been calculated using the spreadsheet of Locock (2014). All Na-clinopyroxenes analysed in both dyke types are aegirine. In GR-II, the core of cpx-I is richer in Ca and Zr (1.0 wt.%

https://doi.org/10.1180/minmag.2017.081.053 Published online by Cambridge University Press

TABLE 3. Average compositions of nacareniobsite-(Ce) and turkestanite in pegmatitic agpaitic (GR-III) dykes.

Mineral	Nacareniobsite-(Ce)		Turkestanite						
	(Fig. 4*a–b*)			Unaltered (Fig. 4*b*)		Altered core (Fig. 4*c–d*)		Rim surrounding altered core (Fig. 4*c–d*)	
n	24	σ		4	σ	5	σ	7	σ
SiO_2	28.70	0.30	SiO_2	51.13	0.20	47.01	1.33	50.15	0.81
Nb_2O_5	13.60	0.70	ThO_2	28.39	1.10	20.87	1.34	27.79	0.57
TiO_2	1.67	0.34	UO_2	1.65	0.18	2.05	0.28	1.92	0.26
La_2O_3	4.52	0.15	Al_2O_3	0.04	0.06	0.85	0.06	0.00	0.01
Ce_2O_3	10.45	0.37	Fe_2O_3	0.19	0.06	0.40	0.15	0.15	0.08
Nd_2O_3	3.86	0.31	La_2O_3	0.15	0.03	0.96	0.21	0.32	0.09
Pr_2O_3	1.11	0.21	Ce_2O_3	0.36	0.14	1.94	0.51	0.85	0.23
Sm_2O_3	0.42	0.21	Nd_2O_3	n.a.	–	n.a.	–	0.18	0.09
Gd_2O_3	0.29	0.29	CaO	9.03	0.18	9.26	0.30	9.28	0.25
Y_2O_3	0.50	0.08	MnO	0.34	0.02	3.18	0.51	0.37	0.32
CaO	19.50	0.52	Na_2O	1.14	0.10	0.41	0.08	1.25	0.17
Na_2O	10.25	0.43	K_2O	2.40	0.03	0.95	0.08	2.41	0.12
F	8.50	0.63							
O = F	3.58	0.27							
Total	99.80	0.88	Total	94.90	0.61	88.04	0.97	94.65	1.21
Formulae based on (O + F) = 18			Formulae based on (Si + Al) = 8						
Si	3.94	0.06	Si	7.99	0.01	7.83	0.01	8.00	0.00
Nb	0.84	0.04	Al	0.01	0.01	0.17	0.01	0.00	0.00
Ti	0.17	0.04	Sum T	8.00	0.00	8.00	0.00	8.00	0.00
Ce	0.52	0.02	Th	1.01	0.04	0.79	0.07	1.01	0.03
La	0.23	0.01	U	0.06	0.01	0.08	0.01	0.07	0.01
Nd	0.19	0.02	Fe^{3+}	0.02	0.01	0.06	0.02	0.02	0.01
Pr	0.06	0.01	*REE*	0.00	0.00	0.09	0.06	0.00	0.00
Sm	0.02	0.01	Sum A	1.09	0.04	1.02	0.03	1.10	0.03
Gd	0.01	0.01	*REE*	0.03	0.01	0.09	0.04	0.07	0.02
Y	0.04	0.01	Ca	1.51	0.03	1.65	0.03	1.59	0.02
Ca	2.87	0.08	Mn	0.00	0.00	0.04	0.01	0.01	0.00
Sr	0.00	0.00	Na	0.35	0.03	0.13	0.02	0.33	0.02
Na	2.73	0.10	Sum B	1.89	0.07	1.92	0.03	1.99	0.02
F	3.68	0.25	Na	0.00	0.00	0.00	0.00	0.06	0.05
			K	0.48	0.00	0.20	0.01	0.49	0.02
			Sum C	0.48	0.00	0.20	0.01	0.55	0.07

Abbreviations: b.d.l. = below detection limit, n.a. = not analysed, σ = standard deviation, *n* = number of analyses.

for both CaO and ZrO_2) than the rim (0.6 wt.% CaO and 0.2 wt.% ZrO_2) whereas the Ti content increases slightly in the rim from 1.1 to 1.6 wt.%. The composition of cpx-II is similar to that of the cpx-I rim. The *REE* distribution patterns have the same appearance in both dyke types although the *REE* concentrations are slightly higher in aegirine from GR-II than in GR-III (Fig. 6*d*). Trace-element distribution patterns are similar, except for Rb, Ba, Th and U, which are all below detection limits in GR-II, and above them in GR-III.

Back-scatter electron images and X-ray element distribution mapping of a cpx-I phenocryst in GR-II illustrate the discontinuous zoning pattern between a homogeneous core and a zoned rim, as well as their compositional differences (Fig. 10). The qualitative X-ray Si map (Fig. 10*b*) shows the distribution of alkali feldspar (orange), clinopyroxene (green), quartz (red) and Zr-minerals (blue).

https://doi.org/10.1180/minmag.2017.081.053 Published online by Cambridge University Press

TABLE 4. Average compositions of aegirine in pegmatitic transitional (GR-II) and pegmatitic agpaitic (GR-III) dykes.

Dyke type	Pegmatitic transitional (GR-II)						Pegmatitic agpaitic (GR-III)	
Mineral	cpx-I-core		cpx-I-rim		cpx-II		aeg	
n	6	σ	5	σ	5	σ	5	σ
SiO_2	52.33	0.14	52.67	0.15	52.68	0.20	52.67	0.16
TiO_2	1.09	0.02	1.60	0.40	1.38	0.70	1.53	0.67
ZrO_2	1.02	0.10	0.21	0.10	0.35	0.15	0.23	0.27
Al_2O_3	0.17	0.02	0.28	0.02	0.27	0.05	0.25	0.04
FeO(c)	7.78	0.40	7.81	0.36	7.96	1.15	6.54	0.73
Fe_2O_3(c)	23.64	0.56	23.54	0.90	23.82	2.36	24.69	1.30
MnO	0.27	0.02	0.37	0.16	0.21	0.07	0.20	0.08
MgO	b.d.l.	–	b.d.l.	–	b.d.l.	–	0.17	0.03
CaO	0.95	0.10	0.59	0.09	0.60	0.10	0.61	0.16
Na_2O	12.13	0.08	12.27	0.12	12.26	0.15	12.54	0.19
K_2O	b.d.l.	–	b.d.l.	–	b.d.l.	–	b.d.l.	–
Total	99.38	0.27	99.34	0.41	99.53	0.30	99.42	0.55
Formulae based on 4 cations and 6 oxygens								
Si	2.034	0.007	2.038	0.008	2.037	0.012	2.032	0.008
Ti	0.032	0.001	0.046	0.012	0.040	0.020	0.044	0.019
Zr	0.019	0.002	0.004	0.002	0.007	0.003	0.004	0.005
Al	0.008	0.001	0.013	0.001	0.012	0.002	0.011	0.002
Fe^{2+}	0.253	0.021	0.253	0.019	0.257	0.051	0.211	0.024
Fe^{3+}	0.691	0.016	0.686	0.024	0.693	0.067	0.717	0.037
Mn	0.009	0.003	0.012	0.006	0.007	0.002	0.006	0.005
Mg	–	–	–	–	–	–	0.009	0.002
Ca	0.040	0.004	0.024	0.004	0.025	0.004	0.025	0.007
Na	0.914	0.005	0.921	0.006	0.920	0.009	0.938	0.010
K	–	–	–	–	–	–	–	–

Abbreviations: aeg = aegirine, cpx = clinopyroxene, b.d.l. = below detection limit, (c) = calculated, σ = standard deviation, *n* = number of analyses.

TABLE 5. Average compositions of amphibole in pegmatitic transitional (GR-II) and pegmatitic agpaitic (GR-III) dykes. Lithium determined by LA-ICP-MS.

Dyke type	Pegmatitic transitional (GR-II)		Pegmatitic agpaitic (GR-III)	
Mineral	fluoro-arfvedsonite		ferri-fluoro-leakeite	
n	10	σ	2	σ
SiO_2	51.12	0.82	54.52	0.03
TiO_2	0.78	0.16	0.37	0.09
ZrO_2	0.19	0.19	n.a.	n.a.
Al_2O_3	0.13	0.06	0.15	0.01
FeO(c)	22.26	1.55	4.06	0.07
Fe_2O_3(c)	10.98	1.58	16.63	0.34
MnO	1.23	0.09	0.90	0.05
ZnO	0.28	0.14	0.44	0.05
MgO	0.04	0.04	7.59	0.08
CaO	0.31	0.07	0.44	0.15
Li_2O	0.64	0.05	1.20	–
Na_2O	8.95	0.28	9.81	0.02
K_2O	1.51	0.30	1.79	0.09
H_2O^+(c)	0.68	0.28	0.00	0.00
F	2.62	0.57	4.72	0.15
Cl	b.d.l.	–	b.d.l.	–
O = F,Cl (c)	−1.10	0.24	−1.99	0.06
Total	100.60	0.89	100.65	0.02
Formulae based on sum Si to K = 16				
Si	7.98	0.05	7.94	0.00
Al	0.01	0.01	0.03	0.00
Ti	0.05	0.04	0.03	0.00
Fe^{3+}	0.01	0.00	0.01	0.00
*Sum T	8.01	0.02	8.00	0.00
Ti	0.08	0.03	0.02	0.00
Zr	0.02	0.01	–	–
Al	0.02	0.01	–	–
Fe^{3+}	1.29	0.18	1.82	0.03
Zn	0.04	0.01	0.05	0.01
Mn^{2+}	0.16	0.01	0.11	0.01
Fe^{2+}	2.91	0.20	0.49	0.01
Mg	0.01	0.01	1.65	0.02
Li	0.40	0.03	0.70	0.00
*Sum C	4.89	0.08	4.83	0.01
Ca	0.05	0.01	0.07	0.02
Na	1.95	0.01	1.93	0.02
*Sum B	2.00	0.00	2.00	0.00
Na	0.76	0.11	0.84	0.03
K	0.30	0.06	0.33	0.02
*Sum A	1.06	0.15	1.17	0.01
OH	0.70	0.29	–	–
F	1.30	0.29	2.00	0.00
Cl	–	–	–	–
*Sum W	2.00	0.00	2.00	0.00
Sum T + C + B + A	15.96	0.10	16.00	0.00

Abbreviations: b.d.l. = below detection limit, (c) = calculated, σ = standard deviation, *n* = number of analyses.
*Sum T is ideally 8 apfu; sum C ideally 5 apfu; sum B ideally 2 apfu; sum A from 0 to 1 apfu; sum W ideally 2 apfu.

https://doi.org/10.1180/minmag.2017.081.053 Published online by Cambridge University Press

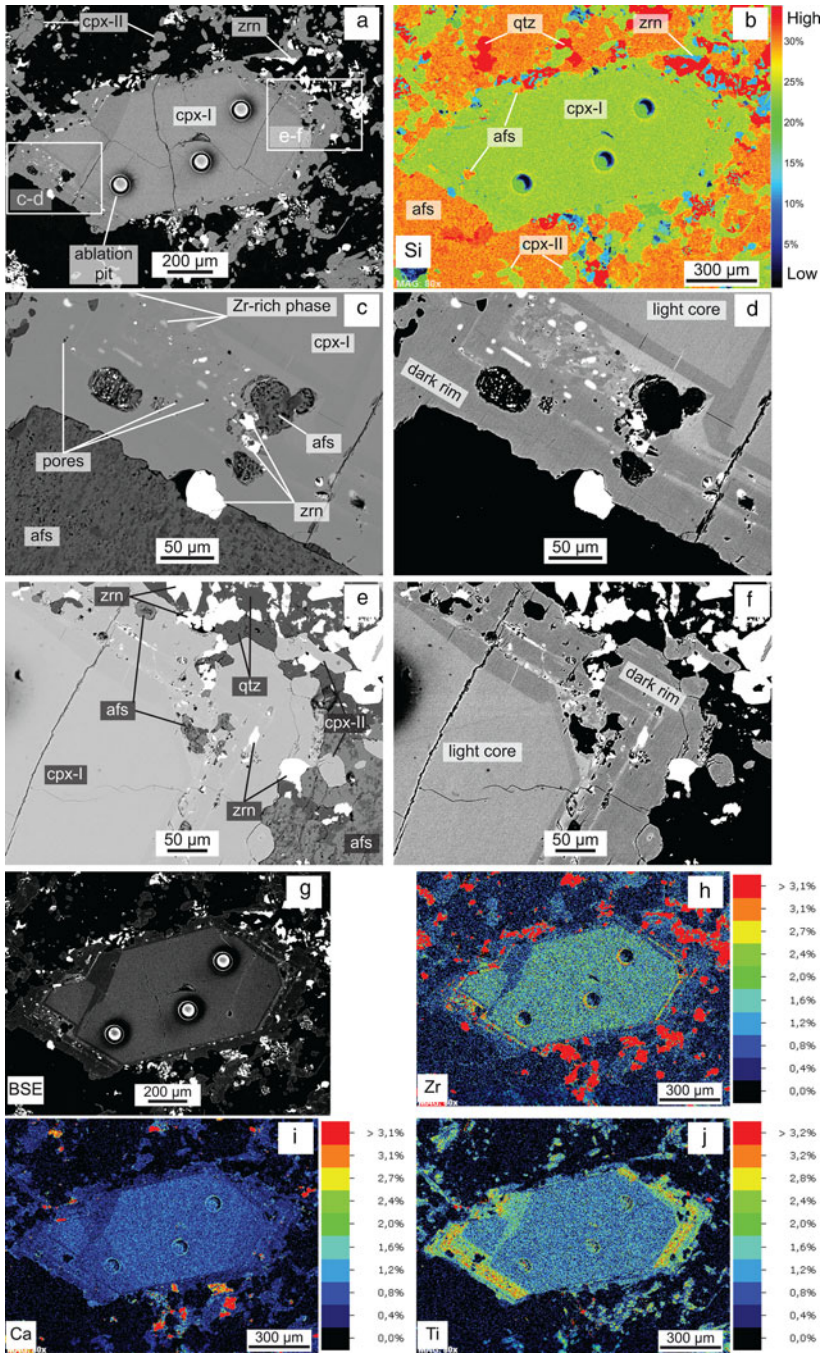

FIG. 10. (*a*) BSE image of zoned clinopyroxene phenocryst (cpx-I) surrounded by small clinopyroxene (cpx-II), zircon, alkali feldspar and quartz; (*b*) false-coloured X-ray map for Si of (*a*); (*c–d*) the left; and (*e–f*) right tips of the clinopyroxene phenocryst in (*a*) with different grey contrast. Band overgrowths contain pores, zircon and alkali feldspar inclusions, and Zr-rich light grey patches. (*g–j*) False-coloured X-ray maps showing the distribution of zirconium (Zr), calcium (Ca) and titanium (Ti). Abbreviations: afs: alkali feldspars; cpx: clinopyroxene, qtz: quartz; zrn: zircon.

https://doi.org/10.1180/minmag.2017.081.053 Published online by Cambridge University Press

The cpx-I shows a homogeneous light grey core enriched in Zr and Ca and depleted in Ti with respect to the external dark rim. This rim is characterized by porous, light and dark grey overgrowths containing inclusions of zircon, alkali feldspar and light grey patches (Fig. 10*c*,*d*,*e*,*f*). These features are restricted to the external rim and do not affect the light core. The light grey patches, porosity and zircon inclusions are mostly restricted to the light grey bands. The composition of zircon and light grey patches has been analysed qualitatively by energy-dispersive spectroscopy. Zircon contains significant concentrations of Ce, Ca, Fe and Al, whereas the light grey patches mainly contain Si, Zr and Na.

Amphiboles in both dyke types are Na-rich, classified using the spreadsheet of Locock (2014) as an arfvedsonite in GR-II and as a ferri-fluoro-leakeite in GR-III. Lithium and fluorine contents in amphibole from GR-III are double those in GR-II. The most significant difference is the very high Mg content (7.6 wt.%) in amphibole from GR-III, which is very low (< 0.1 wt.%) in amphibole from GR-II. Their *REE* distribution patterns have a similar appearance in the *LREE* portion, with a higher content of *LREE* in GR-III than in GR-II, and a *HREE* portion with a steep positive slope in GR-III and a slightly flat curved shape in GR-II (Fig. 6*e*). Their trace-element distribution patterns have minor variations except for U, which is three orders of magnitude more concentrated in GR-III than in GR-II, and the geochemical twins Zr-Hf, which are one order of magnitude more concentrated in GR-II than in GR-III (Fig. 6*e*).

Discussion

Unusual occurrence of EGM in SiO_2-oversaturated rocks

Chlorine solubility in the melt as the main limiting factor for EGM crystallization

The EGM described above are new examples occurring in SiO_2-oversaturated rocks, and add to the list of other complex Na-K-Ca-Zr-silicates occurring in peralkaline granites (Table 1). It is now accepted that the term agpaitic, originally used to designate SiO_2-undersaturated rocks that contain complex Na-K-Ca-Zr-silicates (Sørensen, 1997; Le Maitre *et al.*, 2002), can be extended to SiO_2-oversaturated rocks (Marks *et al.*, 2011). Marks *et al.* (2011) also point out that most Zr minerals occurring in peralkaline granite (e.g. elpidite and dalyite) have a higher molar amount of SiO_2 relative to alkalis and ZrO_2 than Zr minerals in nepheline syenite (e.g. catapleiite and wadeite), due to the higher SiO_2 activity in this type of melt. In addition, Zr minerals in peralkaline granite are either volatile free (e.g. dalyite and vlasovite) or H_2O rich (e.g. elpidite). The EGM, unlike other agpaitic minerals found in peralkaline granites and pegmatites, are rich in Cl. Therefore, in addition to strongly peralkaline conditions and high Zr melt contents, the Cl content of the melt appears to be a critical parameter for crystallization of EGM in peralkaline granites (Sørensen, 1997; Giehl *et al.*, 2014).

Chlorine is considered to be an incompatible element and is thus enriched in most evolved melts, although small amounts can be incorporated in amphibole, mica and apatite (Aiuppa *et al.*, 2009). It has been shown that the fundamental controls on the solubility of Cl in silicate melts include the composition and structure of the melt, pressure and temperature (Signorelli and Carroll, 2002; Oppenheimer *et al.*, 2014). Chlorine solubility in silicic melts increases with decreasing pressure and increasing temperature (Webster, 1992*a*). Chlorine is also known to have a high liquid/melt partition coefficient, leading to depletion of melts in Cl when a fluid phase is exsolved (Webster, 1992*b*). The high capacity of peralkaline melts, and more particularly of agpaitic melts, to retain volatiles and rare elements has been discussed by several authors (e.g. Kogarko, 1974; Metrich and Rutherford, 1992). Several experimental studies have shown that the solubility of Cl in peralkaline SiO_2-oversaturated (pantelleritic) and undersaturated (phonolitic) melts is similar, in agreement with the concentration of Cl measured in natural samples (Metrich and Rutherford, 1992; Signorelli and Carroll, 2000, 2002). However, in granites and nepheline syenites, their intrusive equivalents, the retention of Cl is controlled by the composition of the crystallizing phases and by the eventuality of fluid exsolution. In SiO_2-undersaturated rocks such as nepheline syenite, Cl can be incorporated into the Cl-rich rock-forming mineral sodalite, but in peralkaline granite, there are no major Cl-rich minerals. Furthermore, exsolution of a NaCl-rich fluid phase is common in peralkaline granites and is usually evoked to explain the scarcity of Cl in these rocks (Webster, 1997). Thus, the window for EGM crystallization in SiO_2-oversaturated rocks is rather restricted, requiring a highly evolved peralkaline melt composition and no, or very late, exsolution of a fluid phase. We thus suggest that the scarcity of EGM in peralkaline granites is related to the unavailability of Cl in the melt due to exsolution

https://doi.org/10.1180/minmag.2017.081.053 Published online by Cambridge University Press

of a fluid phase at a late stage of crystallization. In the Ambohimirahavavy complex, we have shown in a previous paper that an orthomagmatic fluid exsolved from the melt at a late stage of crystallization of the peralkaline dykes (Estrade *et al.*, 2015). The interstitial texture of EGM indicates that favourable conditions for its crystallization, i.e. a sufficient amount of Cl and Zr in the melt, were only achieved at the very late magmatic stage. However, these conditions evolved rapidly towards exsolution of an orthomagmatic fluid that partly altered the EGM.

The very unusual association of early magmatic EGM and quartz in the GR-III peralkaline pegmatite

The agpaitic GR-III granite represents the most differentiated lithology in the complex. This is shown by its agpaitic mineralogy and the coexistence of separate grains of albite and K-feldspar, indicating that the temperature of crystallization had decreased to below the feldspar solvus, and contrasts with crystallization of perthitic alkali feldspar in GR-II. These characteristics are attributed to the extremely evolved composition of the melt from which GR-III crystallized, and its extreme enrichment in HFSE, Na and volatiles (Estrade *et al.*, 2014*a*). To our knowledge, the association of early magmatic EGM and quartz in GR-III is the only known example of EGM as an early liquidus phase in granite. However, unlike the other main minerals, quartz is not present as inclusions in EGM, suggesting that quartz probably crystallized late, as is also indicated by its interstitial texture. This raises the question of whether quartz could have crystallized at a post-magmatic stage, i.e. from a hydrothermal fluid. However, the lack of reaction textures between these two minerals, or with any other agpaitic mineral, suggest a magmatic origin for quartz. Indeed, circulation of a hydrothermal fluid among these minerals would have severally affected the very unstable agpaitic minerals. The unusual composition of the GR-III melt compared to GR-II is further shown by the high Mg content of amphibole (Table 5, 8.0 wt.% MgO) and by the high Ca content of all the agpaitic minerals (Tables 2 and 3, 7.7 wt.% in EGM, 19.5 wt.% in nacareniobsite-(Ce) and 9.0 wt.% in turkestanite). High Mg contents, similar to those measured in GR-III, have been reported in ferri-fluoro-leakeite in nepheline syenite pegmatite from the Larvik Plutonic complex in Norway (Oberti *et al.*, 2014) and in the Verkhnee Espe deposit in Kazakhstan (Cámara *et al.*, 2010). However, in the former occurrence, the Mg enrichment is not discussed, whereas in the latter, it is unclear whether the amphibole is magmatic or crystallized at a hydrothermal stage. The high Mg and Ca contents of these minerals contrasts with the composition of agpaitic melts, which are typically highly depleted in Mg – a highly compatible and early fractionating element – and moderately depleted in Ca (Sørensen, 1997). To this effect, Marks *et al.* (2011) have shown that the Ca content of evolved agpaitic melts varies depending on the nature of the parental melt and whether or not plagioclase had fractionated from the melt. The considerably negative Eu anomaly of the whole-rock *REE* patterns for both GR-II and GR-III dyke types (Fig. 6*a*) indicates significant fractionation of plagioclase from their parental melt; thus, the melt from which both dykes crystallized was depleted in Ca, following an evolution similar to the Ca-depleted trend of the Ilímaussaq complex (Marks *et al.*, 2011). And, as far as we know, Mg enrichment has never been documented in alkaline complexes.

A possible explanation for the high Mg and Ca contents in the GR-III melt is contamination of the dykes by the host sediments (marls, mudstone and limestone) during emplacement. It is also possible that some of the Ca could have been introduced during fluid-rock interaction at a post-magmatic stage, such as described at Strange Lake during Ca-metasomatism (Salvi and Williams-Jones, 1996; Gysi *et al.*, 2016; Vasyukova *et al.*, 2016). However, textural evidence clearly rules out a hydrothermal overprint of the primary Ca-bearing agpaitic minerals and Mg-bearing amphibole at Ambohimirahavavy.

The addition of Ca to the GR-III melt by contamination would have had a substantial effect on the solubility of Cl. Indeed, Chevychelov (1999) has shown that the solubility of Cl in a melt correlates positively with its CaO content and with the CaO/SiO_2 molar ratio. Using whole-rock compositional data from our previous studies on pegmatitic dykes, the CaO/SiO_2 ratios are one order of magnitude higher in GR-III (0.053, sample EU01; Estrade *et al.*, 2014*a*) compared with GR-II ($\leq$0.007, samples AM30, AM50 and AM113A; Estrade *et al.*, 2014*b*). Therefore, we propose that the contamination of the highly evolved GR-III melt by Ca-rich material allowed for crystallization of early-magmatic eudialyte by increasing the concentration level of Cl in the melt because fluid

https://doi.org/10.1180/minmag.2017.081.053 Published online by Cambridge University Press

saturation was suppressed. In GR-II, the low Mg content of amphibole and other minerals and the relatively low Ca content in cpx-I and EGM (Tables 2, 4 and 5) may indicate a lower contamination level than for GR-III.

REE and trace elements in EGM

High REE content of EGM

Trace-element patterns of EGM for SiO_2-oversaturated (Ambohimirahavavy, Ascension Island and Straumsvola) and undersaturated (Ilímaussaq and Mont Saint Hilaire) complexes is displayed in Fig. 6*a*. In SiO_2-oversaturated rocks, EGM generally have higher *REE* contents than in SiO_2-undersaturated counterparts. In addition, most of the EGM from SiO_2-undersaturated rocks that have similarly high *REE* contents are reported to be post-magmatic (hatched pattern in Fig. 7), and so probably crystallized from a *REE*-rich fluid (Figs 5*b* and 7). The *REE* enrichment in EGM in GR-II can be explained by the fact that EGM are the only *REE*-bearing minerals in GR-II, and thus scavenged most of the *REE* in the melt. By contrast, in GR-III, nacareniobsite-(Ce) is also a major *REE*-bearing mineral and competed with EGM for the uptake of *REE*. Harris *et al.* (1982; 1987) considered the Ca-poor composition of peralkaline granites from Ascension Island and Straumsvola to explain the *REE* enrichment in EGM. They suggested that, because *REE* are incorporated in the same structural site as Ca in EGM, high amounts of *REE* entered the Ca site to compensate for its paucity in the melt from which the mineral crystallized. The negative correlation between La + Ce + Nd + Y and Ca clearly indicates that these elements compete for the same structural site (Fig. 5*b*). However, although whole-rock Ca contents in GR-II, Ascension Island and Straumsvola are similarly low (0.2 to 0.5 w. %), EGM from Straumsvola are depleted in *HREE* compared to those in the other two localities. Thus, another mechanism must be evoked to explain the difference in *HREE* content.

HREE enrichment in EGM: the role of melt composition

The *HREE* content of the melt can be estimated qualitatively by examining the *REE* distribution patterns of the major minerals present in the rocks (Fig. 6). In GR-II, the major minerals aegirine, amphibole and EGM all show *HREE* enrichments, suggesting that the GR-II melt was enriched in *HREE*. In GR-III, however, all minerals have lower *HREE* concentrations, surely reflecting an overall lower concentration of *HREE* in the GR-III melt. This difference is also evident from the whole-rock *REE* distribution patterns; in GR-II the *HREE* show a flat profile (Gd/Lu = 0.97), whereas it decreases slightly in GR-III (Gd/Lu = 1.73). We have pointed out above that the GR-III dykes are the most evolved lithology in the complex, and that they represent a melt produced by extensive fractionation. We suggest that at a late stage of evolution the *HREE* became compatible due to the abundant crystallization of phases that could incorporate them, such as aegirine and arfvedsonite, and were thus fractionated. The resulting melt, albeit very evolved, was thus relatively depleted in *HREE*.

U and Pb in EGM

Among all trace elements analysed in EGM from both dykes, U and Pb show the most markedly different behaviour (Fig. 6*a*). Uranium concentration in EGM, as for aegirine and amphibole, is higher in GR-III than in GR-II. As proposed for *HREE* above, the opposing behaviour of U in EGM might be attributed to its difference in concentration in the GR-II and GR-III melts. A much higher U concentration in the melt from which GR-III crystallized would be consistent with the presence of turkestanite in this granite, as U is a major constituent of this rare mineral, with up to 2 wt.% UO_2. The higher U concentration in the GR-III melt thus reflects its highly incompatible behaviour, leading to an enrichment in the most evolved melts that were formed by significant fractional crystallization. The opposite observation can be made for Pb, which shows a positive and negative anomaly compared to its neighbouring elements in EGM from GR-II and GR-III, respectively (Fig. 6*a*). This opposite behaviour contrasts with the bulk Pb content, which is similar in both dykes. In GR-II, EGM and K-feldspar are the only minerals that can accommodate significant amounts of Pb, as aegirine and amphibole have very low Pb contents (few ppm to below ppm, see Supplementary material). In GR-III, in addition to EGM and K-feldspar, Pb is easily incorporated into turkestanite (~400 ppm, see Supplementary material). As feldspars are present in similar modal amounts in GR-II and GR-III, we think that they had a similar effect on bulk Pb content of the two melts. Therefore, we attribute the relative low Pb content in EGM from GR-III to its concomitant uptakes by turkestanite.

https://doi.org/10.1180/minmag.2017.081.053 Published online by Cambridge University Press

Destabilization of EGM and post-magmatic assemblage

Alteration of GR-II

The destabilization of EGM and concomitant sudden change in cpx-I composition in GR-II (Figs 8 and 10), together with the local destabilization of the three agpaitic minerals (EGM, nacareniobsite-(Ce) and turkestanite) in GR-III (Fig. 9), indicate that both granites experienced late- to post-magmatic alteration. The occurrence of alteration is a very common feature in peralkaline granites (Salvi and Williams-Jones, 2006; Kynicky *et al.*, 2011; Kempe *et al.*, 2015; Gysi *et al.*, 2016; Vasyukova *et al.*, 2016) and in most cases the primary agpaitic minerals in these rocks undergo complete replacement, to the point that the precursor is not always easy to recognize. Examples include the Strange Lake complex in Canada, where most of the subsolvus granitic facies contain pseudomorphs of gittinsite after a euhedral precursor phase (Birkett *et al.*, 1992; Mariano and Mariano, 2014). Rare occurrences of partial replacement from drill core samples allowed identification of the primary mineral as elpidite, which was transformed to gittinsite via an intermediate step involving armstrongite (Salvi and Williams-Jones, 1995). Other instances of complete pseudomorphism include the Khan Bogd complex (Kynicky *et al.*, 2011) and Khaldzan Buregtey complex (Kempe *et al.*, 2015). Detailed mineralogical studies in some of these localities have shown that destabilization of these agpaitic minerals is a subsolidus process, related either to interaction with external fluids or to the exsolution of a fluid from the melt at a very late stage of crystallization. In some cases, fluid inclusion studies have documented the input of external fluids which may cause formation of relatively rare minerals, as was the case at Strange Lake, where Ca to form gittinsite was derived from a meteoric fluid (Salvi and Williams-Jones, 1990, 1996).

The above discussion indicates that interaction with a fluid, either of orthomagmatic or external origin, at late- to post-magmatic stages is a recurrent phenomenon in agpaitic peralkaline granite. This seems also to be the case in the Ambohimirahavavy complex, as shown in GR-II where secondary assemblages are characterized mainly by the occurrence of pseudomorphs of zircon and quartz after EGM plus an unidentified Ca-zirconosilicate (Fig. 8). Interaction with a fluid is also evidenced by the rims of cpx-I, which show a porous texture associated with zircon inclusions (Fig. 10). A similar texture has been described previously by the authors in zircon in a peralkaline granitic dyke of this complex (Estrade *et al.*, 2014*a*). The association of Zr-rich patches, zircon inclusions and pores in the rim of the cpx-I can be interpreted in terms of coupled dissolution-reprecipitation which occurred at the fluid-cpx-I interface (Putnis, 2009). The presence of Al, Fe and Ca in zircon inclusions, elements that are not compatible in its structure, is further evidence of their hydrothermal origin (Geisler *et al.*, 2007). The fact that the alteration is restricted to the light grey bands in the zoned rims of these crystals is intriguing (Fig. 10*d*, *f*). We suggest that this may be due to their higher content in Zr, thus making them more prone to alteration. The outermost dark rims are poor in Zr and probably precipitated during fluid-rock interaction concomitantly with the small cpx-II grains and late hydrothermal zircon (rich in Ca, Fe and Al) in the groundmass.

We propose that, during the interaction with a fluid, Cl and H_2O were liberated to the fluid phase, causing the destabilization of previously formed EGM and precipitation of zircon and quartz. The elements initially present in EGM were redistributed in the rocks according to their respective mobility in the fluid phase. The precipitation of zircon within the edges of precursor EGM indicates that Zr could not be transported over a long distance. Moreover, Ti could no longer be incorporated in EGM and was therefore incorporated in the crystallizing rims of cpx-I and in the secondary cpx-II crystals (Fig. 10, Table 4). The similar Na_2O content of cpx-I cores and rims indicate that Na activity did not change significantly between magmatic and late- to post-magmatic conditions. The amount of Ca incorporated in secondary phases (mainly in secondary Zr-minerals) could be derived partly from the Ca released in the fluid during the replacement of EGM and cpx-I. However, it is possible that some Ca was added to the system by an external fluid.

Alteration in GR-III is local and Ca-rich

Unlike GR-II, where most of the EGM have been completely replaced, alteration of EGM in GR-III is only a local phenomenon, and most of the EGM are pristine. In the altered parts, the three main agpaitic minerals (EGM, nacareniobsite-(Ce) and turkestanite) are destabilized and replaced, but aegirine and amphibole are mostly preserved. The most significant effect of alteration is the systematic removing of alkalis from the three agpaitic

https://doi.org/10.1180/minmag.2017.081.053 Published online by Cambridge University Press

minerals and the precipitation of Ca-rich phases such as calcite and titanite in secondary assemblages (Fig. 9 and Tables 2 and 3). These observations suggest that, similarly to GR-II, a Ca-rich fluid interacted with GR-III at a late- to post-magmatic stage. The origin of the fluid could be both magmatic and external (Estrade *et al.*, 2015).

Conclusions

We document two new occurrences of EGM in two types of peralkaline granitic dykes from the Ambohimirahavavy complex in northwest Madagascar. We propose that Cl availability is the main limiting factor for the crystallization of EGM in SiO_2-oversaturated rocks. The transitional GR-II granite was produced from a melt that only achieved a sufficient Cl content to crystallize EGM at very late stages, resulting in formation of interstitial EGM. The melt rapidly evolved towards fluid exsolution, losing its Cl and thus hampering EGM crystallization. The resulting orthomagmatic fluid altered the EGM, although only to a limited extent. The agpaitic GR-III granite contains early-formed, abundant EGM. Contamination of the highly evolved GR-III melt by Ca-rich material increased Cl solubility, inducing early EGM crystallization. EGM in these granites have higher *REE* contents than most occurrences in undersaturated complexes. This is explained by the low Ca content of peralkaline melts, which favours *REE* intake in EGM as substitution for Ca. The enrichment of the heavy *REE* in GR-II with respect to EGM in GR-III is a feature inherited from the respective melt compositions, related to fractionation of the more compatible *HREE* in late-forming minerals at late stages of GR-III melt differentiation. In GR-II, exsolution of a NaCl-rich fluid caused destabilisation of EGM and precipitation of zircon and quartz. In GR-III, the exsolving fluid was rich in Ca and produced a calcic alteration assemblage.

Acknowledgements

Financial support for this research was provided by a CESSUR grant from the French Institut National des Sciences de l'Univers to Stefano Salvi, and by the company Tantalus Rare Earth A.G., who also kindly provided access to the Ambohimirahavavy complex and logistical support during fieldwork. We thank Wolfgang Hampel for his invaluable help in the field, Olivier Bruguier for laboratory assistance with the LA-ICP-MS and Sophie Gouy, Philippe De Parseval and Thierry Aigouy for assistance with EPMA and SEM analyses. We are grateful to Roger H. Mitchell and Iain Samson for their constructive and thorough reviews, which helped improve the quality of this manuscript.

Supplementary material

To view supplementary material for this article, please visit https://doi.org/10.1180/minmag.2017.081.053

References

Aiuppa, A., Baker, D.R. and Webster, J.D. (2009) Halogens in volcanic systems. *Chemical Geology*, **263**, 1–18.

Birkett, T.C., Miller, R.R., Roberts, A.C. and Mariano, A. N. (1992) Zirconium-bearing minerals of the Strange Lake intrusive complex, Quebec-Labrador. *The Canadian Mineralogist*, **30**, 191–205.

Borst, A.M., Friis, H., Andersen, T., Nielsen, T.F.D., Waight, T.E. and Smit, M.A. (2016) Zirconosilicates in the kakortokites of the Ilímaussaq complex, South Greenland: Implications for fluid evolution and high-field-strength and rare-earth element mineralization in agpaitic systems. *Mineralogical Magazine*, **80**, 5–30.

Cámara, F., Hawthorne, F.C., Ball, N.A., Bekenova, G., Stepanov, A.V. and Kotel'nikov, P.E. (2010) Fluoroleakeite, $NaNa_2(Mg_2Li)Si_8O_{22}F_2$, a new mineral of the amphibole group from the Verkhnee Espe deposit, Akjailyautas Mountains, Eastern Kazakhstan District, Kazakhstan: description and crystal structure. *Mineralogical Magazine*, **74**, 521–528.

Chevychelov, V.Y. (1999) Chlorine dissolution in fluid-rich granitic melts: The effect of calcium addition. *Geochemistry international*, **37**, 522–535.

Donnot, M. (1963) *Les Complexes Intrusifs Alcalins de la Province Pétrographique d'Ampasindava et leurs Minéralisations*. Bureau des Recherches Géologiques et Minières, Antananarivo.

Estrade, G., Salvi, S., Béziat, D., Rakotovao, S. and Rakotondrazafy, R. (2014*a*) REE and HFSE mineralization in peralkaline granites of the Ambohimirahavavy alkaline complex, Ampasindava peninsula, Madagascar. *Journal of African Earth Sciences*, **94**, 141–155.

Estrade, G., Béziat, D., Salvi, S., Tiepolo, M., Paquette, J.-L. and Rakotovao, S. (2014*b*) Unusual evolution of silica-under- and -oversaturated alkaline rocks in the Cenozoic Ambohimirahavavy Complex (Madagascar): Mineralogical and geochemical evidence. *Lithos*, **206–207**, 361–383.

Estrade, G., Salvi, S., Béziat, D. and Williams-Jones, A.E. (2015) The Origin of Skarn-Hosted Rare-Metal

Mineralization in the Ambohimirahavavy Alkaline Complex, Madagascar. *Economic Geology*, **110**, 1485–1513.

Fleet, S.G. and Cann, J.R. (1967) Vlasovite: a second occurrence and a triclinic to monoclinic inversion. *Mineralogical Magazine*, **36**, 233–241.

Ganzeev, A.A. and Grechishchev, O.K. (2003) A new genetic type of rare-metal alkali granites of Madagascar. *Russian Geology and Geophysics*, **44**, 539–553.

Geisler, T., Schaltegger, U. and Tomaschek, F. (2007) Re-equilibration of zircon in aqueous fluids and melts. *Elements*, **3**, 43–50.

Giehl, C., Marks, M.A.W. and Nowak, M. (2014) An experimental study on the influence of fluorine and chlorine on phase relations in peralkaline phonolitic melts. *Contributions to Mineralogy and Petrology*, **167**, 1–21.

Goodenough, K.M., Schilling, J., Jonsson, E., Kalvig, P., Charles, N., Tuduri, J., Deady, E.A., Sadeghi, M., Schiellerup, H., Müller, A., Bertrand, G., Arvanitidis, N., Eliopoulos, D.G., Shaw, R.A., Thrane, K. and Keulen, N. (2016) Europe's rare earth element resource potential: An overview of REE metallogenetic provinces and their geodynamic setting. *Ore Geology Reviews*, **72**, Part 1, 838–856.

Grew, E.S., Belakovskiy, D.I., Fleet, M.E., Yates, M.G., Mcgee, J.J. and Marquez, N. (1993) Reedmergnerite and associated minerals from peralkaline pegmatite, Dara-i-Pioz, southern Tien Shan, Tajikistan. *European Journal of Mineralogy*, **5**, 971–984.

Guillong, M., Meier, D.L., Allan, M.M., Heinrich, C.A. and Yardley, B.W.D. (2008) SILLS: A MATLAB-based program for the reduction of laser ablation ICP-MS data of homogeneous materials and inclusions. Pp. 328–333 in: *Laser Ablation ICP-MS in the Earth Sciences: Current Practices and Outstanding Issues* (P.J. Sylvester, editor). Mineralogical Association of Canada short course series, Vol. 40. Vancouver, Canada.

Gunter, M.E., Johnson, N.E., Knowles, C.R. and Solie, D. N. (1993) Optical, X-ray, and chemical analysis of four eudialytes from Alaska. *Mineralogical Magazine*, **57**, 743–746.

Gysi, A.P., Williams-Jones, A.E. and Collins, P. (2016) Lithogeochemical vectors for hydrothermal processes in the Strange Lake peralkaline granitic REE-Zr-Nb Deposit. *Economic Geology*, **111**, 1241–1276.

Harris, C. (1983) The petrology of lavas and associated plutonic inclusions of Ascension Island. *Journal of Petrology*, **24**, 424–470.

Harris, C. and Rickard, R.S. (1987) Rare-earth-rich eudialyte and dalyite from a peralkaline granite dyke at Straumsvola, Dronning Maud Land, Antarctica. *Canadian Mineralogist*, **25**, 755–762.

Harris, C., Cressey, G., Bell, J.D., Atkins, F.B. and Beswetherick, S. (1982) An occurrence of rare-earth-rich eudialyte from Ascension Island, south-atlantic. *Mineralogical Magazine*, **46**, 421–425.

Johnsen, O. and Grice, J.D. (1999) The crystal chemistry of the eudialyte group.*Canadian Mineralogist*, **37**, 865–891.

Johnsen, O., Ferraris, G., Gault, R.A., Grice, J.D., Kampf, A.R. and Pekov, I.V. (2003) The nomenclature of eudialyte-group minerals. *Canadian Mineralogist*, **41**, 785–794.

Kabalov, Y.K., Sokolova, E.V., Pautov, L.A. and Schneider, J. (1998) Crystal structure of a new mineral turkestanite: A calcium analogoue of steacyite. *Crystallography Reports*, **43**, 584–588.

Karup-Møller, S. and Rose-Hansen, J. (2013) New data on eudialyte decomposition minerals from kakortokites and associated pegmatites of the Ilímaussaq complex, South Greenland. *Bulletin of the Geological Society of Denmark*, **61**, 47–70.

Karup-Møller, S., Rose-Hansen, J. and Sørensen, H. (2010) Eudialyte decomposition minerals with new hitherto undescribed phases from the Ilímaussaq complex, South Greenland. *Bulletin of the Geological Society of Denmark*, **58**, 75–88.

Kempe, U., Möckel, R., Graupner, T., Kynicky, J. and Dombon, E. (2015) The genesis of Zr–Nb–REE mineralisation at Khalzan Buregte (Western Mongolia) reconsidered. *Ore Geology Reviews*, **64**, 602–625.

Khomyakov, A.P. (1995) *Mineralogy of Hyperagpaitic Alkaline Rocks*. Clarendon Press, Oxford, UK.

Khomyakov, A.P., Dusmatov, V.D., Ferraris, G., Gula, A., Ivaldi, G. and Nechelyustov, G.N. (2003) Zirsilite-(Ce) $(Na,\square)_{12}(Ce,Na)_3Ca_6Mn_3Zr_3Nb(Si_{25}O_{73})(OH)_3(CO)_3{\bullet}H_2O$ and carbolcentbrooksite $(Na,\square)_{12}(Na,Ce)_3Ca_6Mn_3Zr_3Nb(Si_{25}O_{73})(OH)_3(CO_3){\bullet}H_2O$ – two new eudialyte group minerals from Dara-i-Pioz alkaline massif, Tajikistan. *Zapiski Rossiyskogo Mineralogicheskogo Obshchestva*, **132**, 40–51.

Kogarko, L.N. (1974) Role of volatiles. Pp. 474–487 in: *The Alkaline Rocks* (H. Sørensen, editor). John Wiley and Sons, UK.

Kynicky, J., Chakhmouradian, A.R., Xu, C., Krmicek, L. and Galiova, M. (2011) Distribution and evolution of zirconium mineralization in peralkaline granites and associated pegmatites of the Khan Bogd complex, southern Mongolia. *Canadian Mineralogist*, **49**, 947–965.

Lacroix, A. (1915) Sur un type nouveau de roche granitique alcaline, renfermant une eucolite. *Comptes rendus hebdomadaires de l'Académie des sciences*, 253–258.

Lacroix, A. (1923) *Minéralogie de Madagascar, Tome III, lithologie, appendice, index géographique*. Société d'éditions Geographiques, Maritimes et Coloniales, Ancienne Maison Challamel, Paris.

https://doi.org/10.1180/minmag.2017.081.053 Published online by Cambridge University Press

Locock, A.J. (2014) An Excel spreadsheet to classify chemical analyses of amphiboles following the IMA 2012 recommendations. *Computers & Geosciences*, **62**, 1–11.

Le Maitre, R.W., Streckeisen, A., Zanettin, B., Le Bas, M. J., Bonin, B., Bateman, P., Bellieni, G., Dudek, A., Efremova, S., Keller, J., Lameyre, J., Sabine, P.A., Schmid, R., Sørensen, H. and Woolley, A.R. (2002) *Igneous rocks: a classification and glossary of terms*. Cambridge University Press, UK.

Mariano, A.N. and Mariano, A.J. (2014) Cathodoluminescence as a tool in mineral exploration. Pp 97–126 in: *Cathodoluminescence and its Application to Geoscience*. MAC, Short Course 45. Mineralogical Association of Canada, Québec, Canada.

Markl, G., Marks, M. and Frost, B.R. (2010) On the controls of oxygen fugacity in the generation and crystallization of peralkaline melts. *Journal of Petrology*, **51**, 1831–1847.

Marks, M., Hettmann, K., Schilling, J., Frost, B.R. and Markl, G. (2011) The mineralogical diversity of alkaline igneous rocks: critical factors for the transition from miaskitic to agpaitic phase assemblages. *Journal of Petrology*, **52**, 439–455.

Marks, M., Lindhuber, M., Ratschbacher, B., Giehl, C., Nowak, M. and Markl, G. (2015) Eudialyte-Group Minerals as Monitors of Magmatic and Hydrothermal Processes in Peralkaline Rocks. *Goldschmidt Abstracts*. Available at https://goldschmidtabstracts.info/abstracts/abstractView?id=2015001134

McDonough, W.F. and Sun, S.S. (1995) The composition of the earth. *Chemical Geology*, **120**, 223–253.

McLemore, V.T. (2015) Rare Earth Elements (REE) Deposits in New Mexico: Update. *New Mexico Geology*, **37**, 59–69.

Metrich, N. and Rutherford, M.J. (1992) Experimental study of chlorine behavior in hydrous silicic melts. *Geochimica et Cosmochimica Acta*, **56**, 607–616.

Mitchell, R.H. and Liferovich, R.P. (2006) Subsolidus deuteric/hydrothermal alteration of eudialyte in lujavrite from the Pilansberg alkaline complex, South Africa. *Lithos*, **91**, 352–372.

Nockolds, S.R. (1950) On the occurrence of neptunite and eudialyte in quartz-bearing syenites from Barnavave, Carlingford, Ireland. *Mineralogical Magazine*, **29**, 27–33.

Oberti, R., Boiocchi, M., Hawthorne, F.C. and Kristiansen, R. (2014) Ferri-fluoro-leakeite: a second occurrence at Bratthagen (Norway), with new data on Zn partitioning and the oxo component in Na amphiboles. *Mineralogical Magazine*, **78**, 861–869.

Oppenheimer, C., Fischer, T.P. and Scaillet, B. (2014) 4.4 – Volcanic Degassing: Process and Impact. in: *Treatise Geochemistry (Second Edition)* (H.D. Holland and K. Turekian, editors). Elsevier.

Pautov, L.A., Agakhanov, A.A., Sokolova, Y.V. and Kabalov, Y.K. (1997) Turkestanite Th(Ca,Na)2(K1-xx) Si8O20.nH2O – a new mineral with doubled fourfold silicon-oxygen rings. *Zapiski Vserossiyskogo Mineralogicheskogo Obshchestva*, **126**, 45–55.

Pfaff, K., Wenzel, T., Schilling, J., Marks, M. and Markl, G. (2010) A fast and easy-to-use approach to cation site assignment for eudialyte-group minerals. *Neues Jahrbuch für Mineralogie - Abhandlungen*, **187**, 69–81.

Putnis, A. (2009) Mineral replacement reactions. Pp. 87–124 in: *Thermodynamics and Kinetics of Water-Rock Interaction* (E.H. Oelkers and J. Schott, editors). Reviews in Mineralogy & Geochemistry, **Vol. 70**. Mineralogical Society of America and the Geochemical Society, Chantilly, Virginia, USA.

Ratschbacher, B.C., Marks, M.A.W., Bons, P.D., Wenzel, T. and Markl, G. (2015) Emplacement and geochemical evolution of highly evolved syenites investigated by a combined structural and geochemical field study: The lujavrites of the Ilímaussaq complex, SW Greenland. *Lithos*, **231**, 62–76.

Roelofsen, J.N. and Veblen, D.R. (1999) Relationships among zirconosilicates: examination by cathodoluminescence and transmission electron microscopy. *Mineralogy and Petrology*, **67**, 71–84.

Sabine, P.A. (1957) The geology of Rockall, North Atlantic. *Bulletin of the Geological Survey of Great Britain*, **13**, 156–178.

Salvi, S. and Williams-Jones, A.E. (1990) The role of hydrothermal processes in the granite-hosted Zr, Y, REE deposit at strange lake, Quebec Labrador – evidence from fluid inclusions. *Geochimica Et Cosmochimica Acta*, **54**, 2403–2418.

Salvi, S. and Williams-Jones, A.E. (1995) Zirconosilicate phase-relations in the Strange Lake (Lac-Brisson) pluton, Quebec-Labrador, Canada. *American Mineralogist*, **80**, 1031–1040.

Salvi, S. and Williams-Jones, A.E. (1996) The role of hydrothermal processes in concentrating high-field-strength elements in the Strange Lake peralkaline complex, northeastern Canada. *Geochimica et Cosmochimica Acta*, **60**, 1917–1932.

Salvi, S. and Williams-Jones, A.E. (2006) Alteration, HFSE mineralization and hydrocarbon formation in peralkaline igneous systems: Insights from the Strange Lake Pluton, Canada. *Lithos*, **91**, 19–34.

Salvi, S., Fontan, F., Monchoux, P., Williams-Jones, A.E. and Moine, B. (2000) Hydrothermal mobilization of high field strength elements in alkaline igneous systems: Evidence from the Tamazeght complex (Morocco). *Economic Geology*, **95**, 559–576.

Saucier, G., Noreau, C., Casgrain, P., Coté, P., Larochelle, E., Bilodeau, M., Al Hayden, P., Poirier, E., Garon, M., Bertrand, V., Kissiova, M., Mailloux, M., Rougier, M., Camus, Y. and Gagnon, G.

https://doi.org/10.1180/minmag.2017.081.053 Published online by Cambridge University Press

(2013) *NI 43-101 report – Feasibility Study for Kipawa Project*. Matamec Explorations Inc, Quebec, Canada.

Schilling, J., Marks, M., Wenzel, T. and Markl, G. (2009) Reconstruction of magmatic to subsolidus processes in an agpaïtic system using eudialyte textures and composition: a case study from Tamazeght, Morocco. *Canadian Mineralogist*, **47**, 351–365.

Schilling, J., Wu, F.Y., McCammon, C., Wenzel, T., Marks, M., Pfaff, K., Jacob, D.E. and Markl, G. (2011) The compositional variability of eudialyte-group minerals. *Mineralogical Magazine*, **75**, 87–115.

Schmitt, A.K., Trumbull, R.B., Dulski, P. and Emmermann, R. (2002) Zr-Nb-REE mineralization in peralkaline granites from the Amis Complex, Brandberg (Namibia): Evidence for magmatic pre-enrichment from melt inclusions. *Economic Geology and the Bulletin of the Society of Economic Geologists*, **97**, 399–413.

Sheard, E.R., Williams-Jones, A.E., Heiligmann, M., Pederson, C. and Trueman, D.L. (2012) Controls on the concentration of zirconium, niobium, and the rare earth-elements in the Thor Lake Rare Metal Deposit, Northwest Territories, Canada. *Economic Geology*, **107**, 81–104.

Sherer, R.L. (1990) Pajarito yttrium-zirconium deposit, Otero County, New Mexico. *New Mexico Geology*, **12**, 21.

Signorelli, S. and Carroll, M. (2000) Solubility and fluid-melt partitioning of Cl in hydrous phonolitic melts. *Geochimica et Cosmochimica Acta*, **64**, 2851–2862.

Signorelli, S. and Carroll, M. (2002) Experimental study of Cl solubility in hydrous alkaline melts: constraints on the theoretical maximum amount of Cl in trachytic and phonolitic melts. *Contributions to Mineralogy and Petrology*, **143**, 209–218.

Sokolova, E. and Hawthorne, F.C. (2008) From structure topology to chemical composition. V. Titanium silicates: the crystal chemistry of nacareniobsite-(Ce). *Canadian Mineralogist*, **46**, 1333–1342.

Sørensen, H. (1992) Agpaitic nepheline syenites – a potential source of rare elements. *Applied Geochemistry*, **7**, 417–427.

Sørensen, H. (1997) The agpaitic rocks – an overview. *Mineralogical Magazine*, **61**, 485–498.

Vasyukova, O., Williams-Jones, A.E. and Blamey, N.J.F. (2016) Fluid evolution in the Strange Lake granitic pluton, Canada: Implications for HFSE mobilisation. *Chemical Geology*, **444**, 83–100.

Vilalva, F.C.J. and Vlach, S.R.F. (2010) Major- and trace-element composition of REE-rich turkestanite from peralkaline granites of the Morro Redondo Complex, Graciosa Province, south Brazil. *Mineralogical Magazine*, **74**, 645–658.

Vilalva, F.C.J., Vlach, S.R.F. and Simonetti, A. (2013) Nacaraniobsite-(Ce) and britholite-(Ce) in peralkaline granites from the Morro Redondo complex, Graciosa province, southern brazil: occurence and compositional data. *Canadian Mineralogist*, **51**, 313–332.

Webster, J. (1992*a*) Fluid-melt interactions involving Cl-rich granites: Experimental study from 2 to 8 kbar. *Geochimica et Cosmochimica Acta*, **56**, 659–678.

Webster, J.D. (1992*b*) Water solubility and chlorine partitioning in Cl-rich granitic systems: Effects of melt composition at 2 kbar and 800 °C. *Geochimica et Cosmochimica Acta*, **56**, 679–687.

Webster, J.D. (1997) Exsolution of magmatic volatile phases from Cl-enriched mineralizing granitic magmas and implications for ore metal transport. *Geochimica et Cosmochimica Acta*, **61**, 1017–1029.

https://doi.org/10.1180/minmag.2017.081.053 Published online by Cambridge University Press